

The hydrodynamics of a moving fluid-liquid contact line

Citation for published version (APA):

Zanden, van der, A. J. J. (1993). *The hydrodynamics of a moving fluid-liquid contact line*. [Phd Thesis 1 (Research TU/e / Graduation TU/e), Applied Physics and Science Education]. Technische Universiteit Eindhoven. <https://doi.org/10.6100/IR389100>

DOI:

[10.6100/IR389100](https://doi.org/10.6100/IR389100)

Document status and date:

Published: 01/01/1993

Document Version:

Publisher's PDF, also known as Version of Record (includes final page, issue and volume numbers)

Please check the document version of this publication:

- A submitted manuscript is the version of the article upon submission and before peer-review. There can be important differences between the submitted version and the official published version of record. People interested in the research are advised to contact the author for the final version of the publication, or visit the DOI to the publisher's website.
- The final author version and the galley proof are versions of the publication after peer review.
- The final published version features the final layout of the paper including the volume, issue and page numbers.

[Link to publication](#)

General rights

Copyright and moral rights for the publications made accessible in the public portal are retained by the authors and/or other copyright owners and it is a condition of accessing publications that users recognise and abide by the legal requirements associated with these rights.

- Users may download and print one copy of any publication from the public portal for the purpose of private study or research.
- You may not further distribute the material or use it for any profit-making activity or commercial gain
- You may freely distribute the URL identifying the publication in the public portal.

If the publication is distributed under the terms of Article 25fa of the Dutch Copyright Act, indicated by the "Taverne" license above, please follow below link for the End User Agreement:

www.tue.nl/taverne

Take down policy

If you believe that this document breaches copyright please contact us at:

openaccess@tue.nl

providing details and we will investigate your claim.

The Hydrodynamics of a Moving Fluid-Liquid Contact Line

PROEFSCHRIFT

ter verkrijging van de graad van doctor aan de
Technische Universiteit Eindhoven, op gezag van
de Rector Magnificus, prof. dr. J.H. van Lint,
voor een commissie aangewezen door het College
van Dekanen in het openbaar te verdedigen op
dinsdag 5 januari 1993 te 16.00 uur

door

Antonius Johannes Joseph van der Zanden
geboren te Helmond

Dit proefschrift is goedgekeurd door de promotoren

prof. dr. A.K. Chesters

en

prof. dr. ir. L. van Wijngaarden

Contents

1.	<i>Introduction</i>	
1.	Static contact angles	1
2.	Dynamic contact angles	1
3.	Thesis overview	2
2.	<i>An approximate analytical solution of the hydrodynamic problem associated with an advancing liquid-gas contact line</i>	
1.	Introduction	3
2.	The shape of an advancing meniscus between plane-parallel plates	5
3.	The shape of an advancing meniscus in a capillary	8
4.	The numerical solution of the meniscus equation in the plane case	9
5.	The numerical solution of the meniscus equation in the axi-symmetric case	11
6.	Comparison with complete numerical solution	11
7.	Approximate analytical solution of the meniscus equation in the wall region	14
8.	Analytical approximation for the entire meniscus	22
9.	Comparison with experimental results	24
10.	System-dependence of the dynamic contact angle	29
11.	Conclusions and final discussion	29
3.	<i>An approximate solution of the hydrodynamic problem associated with receding liquid-gas contact lines</i>	
1.	Introduction	31
2.	The differential equations describing receding menisci	33

3.	Solution of the meniscus equation	35
4.	Dynamic contact angles	38
5.	The local-wedge approximation	40
6.	Dynamic contact angle dependence on system scale and true contact angle	42
7.	Comparison with experimental results	42
8.	Final discussion	45
4.	<i>An approximate solution of the hydrodynamic problem associated with moving liquid-liquid contact lines</i>	
1.	Introduction	46
2.	The equation governing a steadily moving meniscus between two viscous liquids	48
3.	Solutions of the governing equation	51
4.	The transition to purely advancing or receding behaviour	56
5.	Comparison with numerical solutions	56
6.	Comparison with experimental results	60
7.	Conclusion & discussion	60
5.	<i>Experimental determination of advancing and receding dynamic contact angles in a capillary tube</i>	
1.	Introduction	63
2.	Experiments	64
3.	Results	65
4.	Discussion	68

6.	<i>Experimental determination of the meniscus curvature in the vicinity of an advancing liquid–gas contact line</i>	
1.	Introduction	69
2.	Experimental set–up	70
3.	Measuring procedures	73
4.	Results	75
5.	Discussion and conclusion	78
7.	<i>Conclusion & final remarks</i>	81
	Appendix A	83
	Appendix B	84
	Appendix C	85
	Appendix D	86
	Appendix E	87
	Appendix F	88
	References	90
	Summary	93
	Samenvatting	95
	Curriculum Vitae	97
	Nawoord	98

CHAPTER 1 – *Introduction*

1.1 Static contact angles

Where a static fluid–liquid interface intersects a solid surface a static contact line is formed. The angle between the fluid–liquid interface and the solid surface is the static contact angle φ_s . In the ideal case of pure fluids and a smooth homogeneous surface and provided the system length scale (pore diameter, drop diameter,...) is much larger than the range of intermolecular forces, φ_s is purely a material property. Its value is related to the interfacial tensions (/energies) involved by the Young equation [see, for example, de Gennes (1985)]:

$$\sigma_{12} \cos \varphi_s = \sigma_{23} - \sigma_{13} , \quad \{1.1\}$$

where σ_{ij} are the tensions of the interfaces involved (figure 1.1).

In practice, however, the static contact angle does not exhibit a unique value, but varies between an upper limit (the advancing contact angle) and a lower limit (the receding contact angle). This contact angle hysteresis is known to be caused by roughness or heterogeneity of the solid surface [see, for example, de Gennes (1985)].

By way of qualification, it should be mentioned that extremely close to the line – within the range of intermolecular forces – the meniscus inclination is predicted to deviate somewhat from φ_s [see, for example, de Gennes, Hua & Levinson (1990) or Merchant & Keller (1992)]. For all practical purposes however, this region may be ignored.

1.2 Dynamic contact angles

When a contact line moves over a solid surface, the macroscopically observed angle

differs from its static value. In the past decades it has been shown theoretically and numerically that a large part of this change in the angle is apparent rather than real. Viscous forces in the fluids cause the fluid-liquid interface to exhibit large curvatures very close to the contact line. This deviation from the macroscopic profile cannot be observed with the naked eye.

1.3 Thesis overview

The hydrodynamics associated with an advancing contact line, where a viscous liquid displaces a fluid with a negligible viscosity, is examined in chapter 2. A model is proposed which approximates the shape of an advancing meniscus in a tube or between parallel plates. Comparison of the predictions of the model with available numerical and experimental results provides an indication of its reliability. This model is applied in chapter 3 to receding contact lines, where a viscous liquid is displaced by a fluid of negligible viscosity. In chapter 4 the model is extended to examine moving liquid-liquid contact lines where the viscosity of neither fluid can be neglected. Chapter 5 presents experiments concerning the macroscopic shape of a meniscus in a tube while chapter 6 contains experiments which lay claim to be able to peep into the microscopic region close to the contact line not accessible with the naked eye.

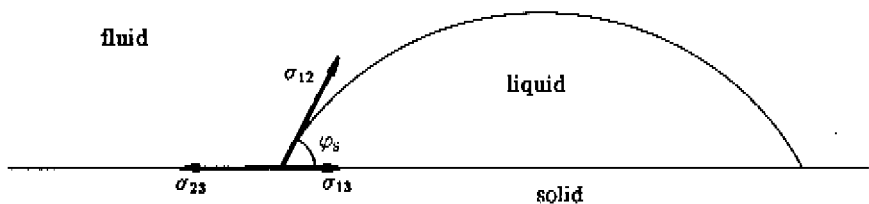


fig 1.1 The static contact angle of a sessile drop of a pure liquid on a smooth homogeneous surface obeys the Young equation.

CHAPTER 2 — *An approximate analytical solution of the hydrodynamic problem associated with an advancing liquid-gas contact line*

2.1 Introduction

It is appealing to extend the concept of contact angle to the dynamic case, in which the three-phase line moves over the solid and the "dynamic" contact angle in the advancing fluid is observed to be an increasing function of the line speed. Even in the simplest case, considered here, of a viscous liquid steadily displacing a gas, one of the problems encountered is that whatever the value of the dynamic contact angle the associated flow field proves to be singular, the pressure in the liquid decreasing without limit as the line is approached if the "classical" approximations of fluid mechanics are retained: that the liquid is a continuum, possessing a surface tension and subject to no slip with respect to the solid. This dilemma does, however, provide the first clue as to the origin of the dynamic contact angle, namely that at least part of the deviation from the static angle must be apparent rather than real, resulting from deformation of the meniscus in a microscopic region close to the line where the pressure in the advancing fluid is very low (for relatively recent reviews, see Dussan V., 1979, de Gennes, 1985 and Blake, 1993). The problem of the singularity remains, however, the magnitude of the deviation from the static angle being unlimited if the classical approximations are retained. It thus appears that the breakdown of one or more of these approximations extremely close to the wall must be taken into account in any complete description of the phenomena.

Even aside from the question of the appropriate wall boundary conditions, the problem of finding the meniscus shape is a difficult one and most solutions to date are based on perturbation techniques, valid only for small values of the capillary number, $\mu U/\sigma$

(μ dynamic viscosity of the liquid, U line speed, σ surface tension): Hansen & Toong (1971b), Voinov (1976), Huh & Mason (1977), Greenspan (1978), Voinov (1978), Kafka & Dussan (1979), Neogi & Miller (1982), Hocking & Rivers (1982), Cox (1986), Hocking (1992). Direct numerical (finite-element) solutions up to a capillary number of almost 10^{-1} have, however, been obtained by Lowndes (1980). Of the preceding authors, all but Voinov coped with the wall boundary condition by assuming the no-slip approximation to break down while retaining the continuum description and the idealization of surface tension. In addition, they assumed the true contact angle to remain unchanged and equal to the static value. Lowndes' results exhibited good agreement with the dynamic contact angles measured by Hoffman (1975) if the size of the region in which slip was significant was taken to be of the order of a molecular dimension (1 nm). This result suggests of course that non-continuum effects are likely to be significant, if not dominant. Another indication towards the breakdown of continuum hydrodynamics at the contact line can be found in the results of molecular dynamics studies of Thompson & Robbins (1989, 1990). Their computations show that close to the contact line there exists a discrepancy between the stress on the solid surface as predicted for a Newtonian fluid (proportional to the velocity gradient) and as computed with the molecular dynamics approach, and this suggests a breakdown of local hydrodynamics. It is not surprising that a continuum theory which averages properties over many molecules fails when the length scale involved is molecular.

The aim of this chapter is to develop an alternative approximation to perturbation techniques for the solution of the advancing meniscus shape in that domain of the wall region in which the classical approximations apply. The approach (Boender, Chesters & van der Zanden, 1991) is based on the solution of the creeping flow and pressure field in the case of a free surface of constant inclination (Moffatt, 1964). This solution should be locally applicable, even at large values of the capillary number, provided the actual inclination changes only slowly (in some appropriate dimensionless sense), much as the Poiseuille equation for pressure drop in a tube would be, provided the tube diameter changed slowly.

This approach yields a second-order ordinary differential equation for the meniscus shape which can either be solved numerically or, with the help of suitable further approximations, analytically.

To make use of the resulting meniscus equation to predict dynamic contact angles some assumption is again required as to the wall boundary condition. In contrast with preceding authors, excepting Voinov, the possibility is explored that the continuum, rather than the no-slip, approximation must be abandoned. Specifically, the classical approximations are supposed to apply up to a distance from the wall of the order of a molecular dimension, at which point the wall has been reached and with it the true contact angle. Like previous authors, the simplest assumption is made regarding the true contact angle -- that this angle remains unchanged and equal to its static value. This assumption, which has been challenged by various authors (for example Hoffman, 1983), is not however as critical as it might seem, since even a considerable line-speed-dependence of the true angle proves hardly to affect the dynamic angle in the advancing case.

2.2 The shape of an advancing meniscus between plane-parallel plates

The stream function Ψ of a creeping liquid flow in a plane wedge, with a constant velocity U prescribed on one boundary and a free surface (zero shear stress) on the other, has been given by Moffatt (1964), in the coordinates θ and ρ , as

$$\Psi = U \rho \frac{\theta \cos \theta \sin \alpha - \alpha \cos \alpha \sin \theta}{\sin \alpha \cos \alpha - \alpha} , \quad [2.1]$$

where α is the angle of the wedge (see figure 2.1). The corresponding deviatoric component of the normal stress in the liquid at the free surface is readily shown to be zero (see appendix A), while the pressure p in the liquid varies along the free surface as (see appendix B)

$$\frac{dp}{d\rho} = \frac{\mu U A(\alpha)}{\rho^2} , \quad [2.2]$$

where μ is the viscosity of the liquid and

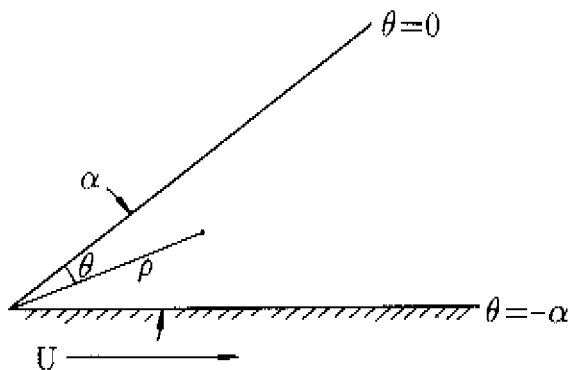


fig 2.1 Viscous flow in a plane wedge bounded by a solid with velocity U ($\theta = -\alpha$) and a free surface ($\theta = 0$).

$$\Lambda(\alpha) = \frac{-2 \sin \alpha}{\sin \alpha \cos \alpha - \alpha} \quad [2.3]$$

An advancing meniscus between two parallel plates may be described by the coordinates r and φ (figure 2.2). In this case the wedge angle φ is not constant but varies along the

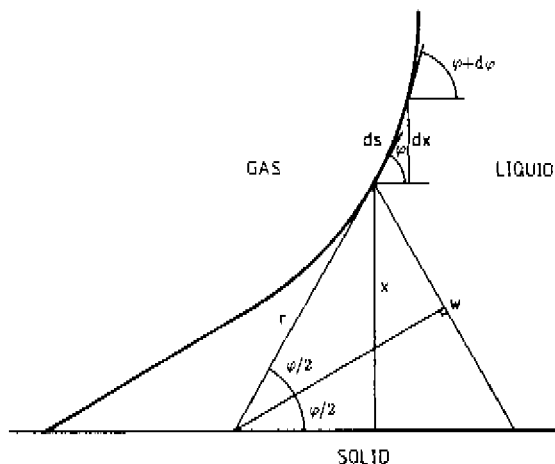


fig 2.2 Definition of variables for an advancing meniscus.

meniscus. However, provided that the stresses exerted by the receding gas on the liquid are negligible (aside from a uniform pressure, taken for simplicity to be zero), the flow is assumed locally to resemble that in a plane wedge (with $\alpha = \varphi$). More precisely, the pressure gradient dp/ds (where s denotes arc length along the meniscus) will be approximated by the pressure gradient $dp/d\rho$ at the free surface of the corresponding plane wedge:

$$\frac{dp}{ds} = \frac{\mu U A(\varphi)}{r^2}. \quad [2.4]$$

Denoting the distance to the wall by x (figure 2.2), [2.4] may be rewritten as

$$\frac{dp}{dx} = \frac{\mu U A(\varphi) \sin \varphi}{x^2}. \quad [2.5]$$

The normal stress, $-p$, exerted by the liquid, is balanced by the surface tension σ , according to Laplace's law:

$$-p = \frac{\sigma}{R} = \sigma \frac{d\varphi}{ds} = \sigma \sin \varphi \frac{d\varphi}{dx}, \quad [2.6]$$

where R is the radius of curvature of the meniscus (reckoned positive if the centre of curvature lies on the gas side). The derivative of [2.6] substituted in [2.5] now gives

$$\frac{1}{A(\varphi) \sin \varphi} \frac{d}{dx} (\sin \varphi \frac{d\varphi}{dx}) = \frac{-Ca}{x^2}, \quad [2.7]$$

in which Ca is the capillary number;

$$Ca = \frac{\mu U}{\sigma}. \quad [2.8]$$

The description of the shape of a moving meniscus between parallel planes by the ordinary differential equation [2.7] is as good as approximation [2.4]. The first correction to this approximation would involve some dimensionless local curvature of the wedge, for example $(d\varphi/\varphi)/(ds/w)$, where w denotes the local wedge width (figure 2.2). Accordingly, [2.4] may be expected to be acceptable provided

$$\frac{d\varphi/\varphi}{ds/w} \ll 1. \quad [2.9]$$

2.3 The shape of an advancing meniscus in a capillary

Unlike the case of parallel plates, the flow behind an advancing meniscus in a capillary tube is no longer two-dimensional, though close to the wall (the region where viscous stresses make the meniscus deviate noticeably from a sphere) [2.5] still provides a good description of the pressure gradient. Because the meniscus is no longer cylindrical, the pressure behind the advancing meniscus is balanced by two radii of curvature:

$$-p = \sigma \left(\frac{1}{R_1} + \frac{1}{R_2} \right), \quad [2.10]$$

where R_1 is the radius of curvature in the plane of figure 2.3 and R_2 in the plane normal to it; R_1 is given (as in [2.6]) by

$$\frac{1}{R_1} = \sin \varphi \frac{d\varphi}{dx}, \quad [2.11]$$

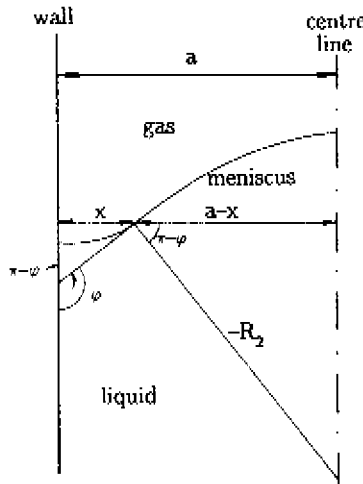


fig 2.3 *Advancing meniscus in a capillary of radius a.*

and R_2 by:

$$\frac{a-x}{-R_2} = \cos(\pi-\varphi) = -\cos \varphi, \quad [2.12]$$

where a is the tube radius (see figure 2.3). From [2.5], [2.10], [2.11] and [2.12] the new

meniscus equation is obtained:

$$\frac{d}{dx} \left(\sin \varphi \frac{d\varphi}{dx} + \frac{\cos \varphi}{a-x} \right) = \frac{-Ca}{x^2} \frac{A(\varphi) \sin \varphi}{x} . \quad [2.13]$$

2.4 The numerical solution of the meniscus equation in the plane case

Equation [2.7] cannot be valid for all x , since this equation is based on [2.1] and [2.6], which treat the liquid as a continuum, bounded by an infinitesimally thin surface possessing a tension. While this is an acceptable approximation on a macroscopic and microscopic scale, on a 'nano scopic' scale, of the order of molecular dimensions, it is certainly not. The distance from the wall beneath which [2.7] is no longer valid will be denoted by λ .

Defining the logarithmic scale of distance

$$\xi = \ln(x/\lambda) , \quad [2.14]$$

[2.7] becomes

$$\frac{1}{A(\varphi) \sin \varphi \lambda \exp(\xi)} \frac{d}{d\xi} \left(\sin \varphi \frac{d\varphi}{\lambda \exp(\xi)} \frac{d\xi}{d\xi} \right) = \frac{-Ca}{\lambda^2 \exp(2\xi)} , \quad [2.15]$$

while the boundary conditions to be satisfied become

$$\varphi = 90^\circ, \text{ at the channel centre } (\xi = \xi_c = \ln[a/\lambda]) , \quad [2.16a]$$

and

$$\varphi = \varphi_0, \text{ at "the wall" } (\xi = 0) , \quad [2.16b]$$

where a denotes the half-width of the channel and the appropriate values of φ_0 and λ in any given system are at present unknown. Equation [2.15] is now written as two first-order differential equations:

$$\frac{d\varphi}{d\xi} = \eta \quad [2.17]$$

and

$$\frac{d\eta}{d\xi} = -Ca \frac{A(\varphi)}{\lambda} + \eta - \frac{\eta^2}{\tan \varphi} . \quad [2.18]$$

Equations [2.17] and [2.18] are integrated numerically in parallel using a second-order

finite-difference scheme and proceeding from assigned values of φ and η at either the wall or the centre plane of the channel (see appendix C). The step size is automatically adjusted to keep the truncation errors in the values of $\Delta\eta$ and $\Delta\varphi$ below any required value (typically 10^{-3} %). The initial value of η is then adjusted in iterative integrations to satisfy the condition at the second boundary. In figure 2.4 three solutions of the meniscus equation [2.7] are presented ($Ca = 0.1$). When integrating from the wall outward it is seen

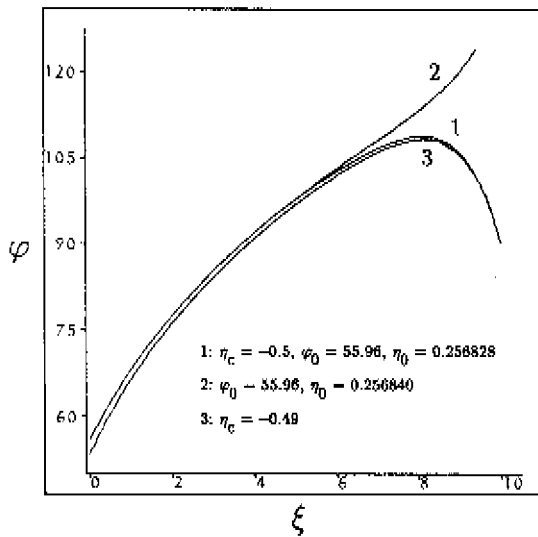


fig 2.4 *Influence of initial curvature, η , on the shape of the meniscus between parallel plates for $Ca = 10^{-1}$ (η_0 -curvature at the wall, η_c -curvature at the centre).*

from curves 1 and 2, with initial η_0 -values of 0.256828 and 0.256840, that the shape of the meniscus far from the wall is highly sensitive to the initial value of η_0 . When integrating towards the wall it appears from curves 1 and 3, with initial η_c -values of -0.5 and -0.49 , that the meniscus shape is much less sensitive to the initial η_c -value. Although the relative difference between the initial values of η is much greater in the latter case than in the preceding one, the difference in the shape of the meniscus is smaller, corresponding to a

difference in φ_0 of only 2° . It can be concluded that the shape of a moving meniscus close to a contact line is rather insensitive to the exact outer boundary conditions. This point is discussed further in section 2.10.

2.5 The numerical solution of the meniscus equation in the axis-symmetric case

Using, again, the logarithmic scale, [2.13] becomes

$$\frac{d}{\lambda \exp \xi} \left(\sin \varphi \frac{d\varphi}{\lambda \exp \xi} + \frac{\cos \varphi}{\lambda (\exp \xi_c - \exp \xi)} \right) = \frac{-Ca A(\varphi) \sin \varphi}{\lambda^2 \exp(2\xi)}. \quad [2.19]$$

This differential equation, describing an advancing meniscus in a tube, can again be written as two first-order differential equations:

$$\frac{d\varphi}{d\xi} = \eta \quad [2.20]$$

and

$$\frac{d\eta}{d\xi} = -Ca A(\varphi) + \eta - \frac{\eta^2}{\tan \varphi} + \frac{\eta \exp \xi}{\exp \xi_c - \exp \xi} - \frac{\exp(2\xi)}{\tan \varphi (\exp \xi_c - \exp \xi)^2}. \quad [2.21]$$

These equations are integrated numerically as in the plane case. The results obtained are compared below with the complete numerical solutions of Lowndes (1980).

The numerical solution in the tube geometry is furthermore compared with the corresponding solution in the plate geometry (figure 2.5). The difference is very small in this case where $Ca = 1$. For smaller Ca -values the differences may be expected to be still smaller and for $Ca = 0$ there will be no difference.

2.6 Comparison with complete numerical solutions

The shape of an advancing meniscus in a capillary has been computed for a number of cases by Lowndes (1980) using a finite-element method. In figure 2.6 the largest- Ca

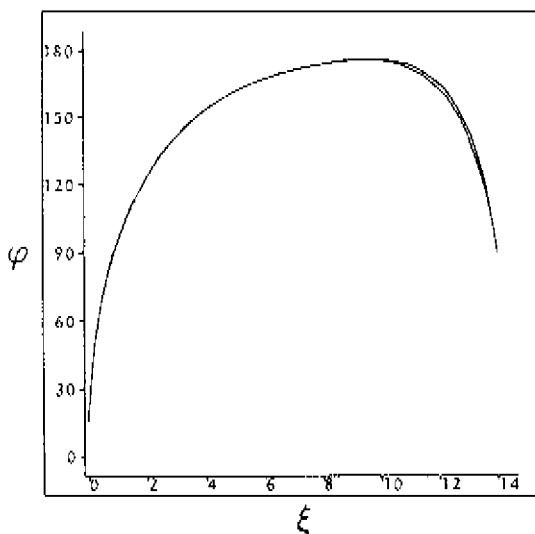


fig 2.5 Comparison of the meniscus profiles in the tube and parallel-plate cases ($Ca = 1$, $\xi_c = 14$, $\varphi_0 = \theta^0$).

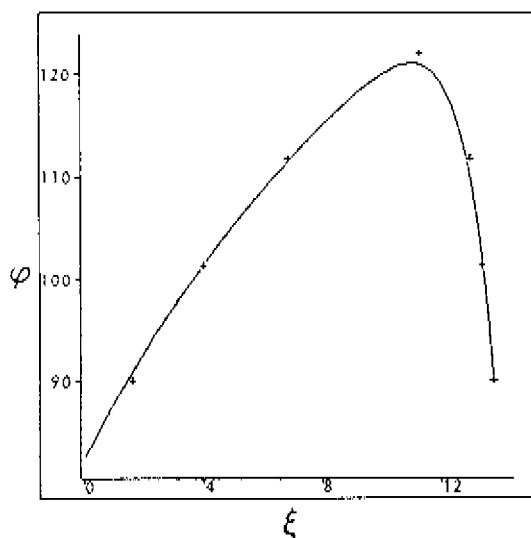


fig 2.6 Comparison of the solution of the axi-symmetric meniscus equation [2.13] (—) with the results obtained by Lowndes (+) for the highest Ca investigated ($Ca = 7.59 \cdot 10^{-2}$).

case treated by Lowndes is compared with the results obtained by integration of [2.19] from the tube axis to the wall. The value of η at the axis has been chosen to optimize the agreement with the results obtained by Lowndes.

Before commenting on the comparison, a word must be said about the boundary conditions used by Lowndes. As noted earlier, Lowndes assumed the continuum and surface-tension approximations to be valid up to the solid surface ($x = 0$) but the liquid-solid no-slip approximation to break down at a distance (the "slip length") of order 10^{-9} m from the contact line. At values of x less than or of the order of the slip length the solution obtained by Lowndes may therefore be expected to deviate appreciably from that based on a no-slip condition and, accordingly, agreement with the meniscus equation [2.19] is no longer to be expected. For this reason, λ was chosen for the purposes of comparison to be 10^{-9} m, resulting in a ξ_c -value of 13.79 for the tube concerned ($a=0.978$ mm).

The two meniscus shapes are in good agreement, with maximum differences of the order of a degree. In the smaller-Ca cases of Lowndes the similarity is comparable or better.

The preliminary conclusion is therefore that the local-wedge approximation looks very promising, implying that the requirement [2.9] is satisfied. This is broadly confirmed by the results obtained which indicate that the dimensionless wedge-angle variation rate, $|(d\varphi/\varphi)/(ds/w)|$, is $\ll 1$ over the greater part of the meniscus for all values of Ca (figure 2.7). Very close to the wall the local-wedge approximation is evidently poor for moderate or large Ca. However, this region constitutes only a small part of the zone in which the meniscus is seriously perturbed from the spherical. Very close to the axis, the wedge approximation is also poor but this is immaterial except at large Ca, viscous stresses in this region being negligible anyway. The problem of modelling the central region at large Ca is discussed in section 2.9.

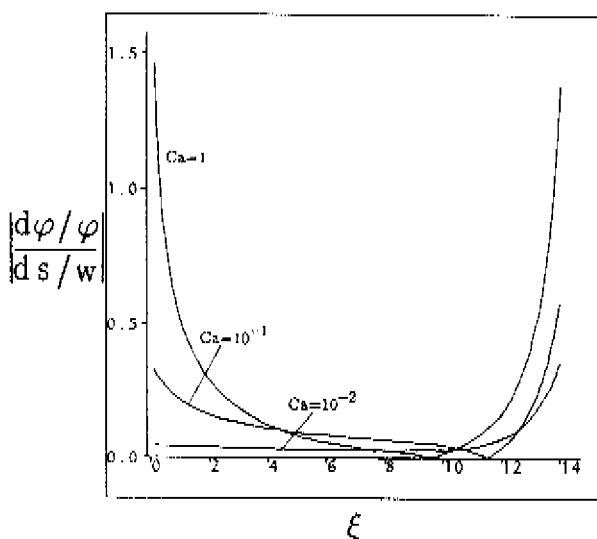


fig 2.7 The dimensionless wedge-angle variation rate $\left| (d\varphi/\varphi)/(ds/w) \right|$ as a function of ξ for $Ca = 1, 10^{-1}$ and 10^{-2} ($\xi_c = 14$ and $\varphi_0 = 45^\circ$).

2.7 Approximate analytical solution of the meniscus equation in the wall region

As the wall is approached the plane meniscus equation [2.7] must always become a good approximation, whether the system geometry is plane or not. This follows from the continual decrease in pressure implied by [2.5], requiring a corresponding increase in curvature in the plane of flow, that in the perpendicular plane being limited to values less than, or of the order of, the reciprocal of the system length scale, [2.12].

In the present section an approximate analytical solution of [2.7] is derived for this region, inspired by its solution in two limiting cases. The first and most obvious of these cases is that of small Ca when the meniscus deviates only slightly from a plane wedge and perturbation approaches are applicable. An analysis of the error in this approximation, however, provides a clue to the second case: that of large φ -values. Both solutions,

furthermore, prove to be covered by the same expression.

The final step is to adopt this expression as an approximate solution in all cases, the reasoning being as follows. Large values of Ca provoke large values of φ over most of the wall region so that the large- φ solution is likely to provide a good approximation in this case too. This means, however, that a single expression provides a good approximation in both the large- and small-Ca limits and this expression is then likely to be a good approximation in the intermediate-Ca range as well.

Clearly, the final test is a comparison of the analytical approximation with exact solutions of [2.7] in the wall region and this test is carried out after the derivations concerned.

The small-Ca limit

Equation [2.7] is based on [2.5], which gives the pressure, p , in the wall region as

$$p(x) = \int_{\chi=x}^{\chi=x_t} \frac{dp}{d\chi} d\chi + p_t = \int_x^{x_t} \frac{\mu UA(\varphi) \sin \varphi}{\chi^2} d\chi + p_t, \quad [2.22]$$

where x_t denotes the largest value of x at which [2.7] is still an adequate approximation and p_t is the corresponding pressure. In view of the strong χ -dependence of the integrand only the region close to $\chi = x$ contributes strongly to the integral and for sufficiently small values of Ca, φ is virtually constant there. In the small-Ca limit, [2.22] therefore simplifies to

$$p(x) = -\mu UA(\varphi) \sin \varphi \left(\frac{1}{x} - \frac{1}{x_t} \right) + p_t, \quad [2.23]$$

which in turn simplifies to

$$p(x) = -\mu UA(\varphi) \sin \varphi / x \quad [2.24]$$

for sufficiently small x .

Combination of [2.6] and [2.24] now leads to

$$\frac{d\varphi}{dx} = \frac{Ca}{x} \frac{A(\varphi)}{x}, \quad [2.25]$$

a result also derived by Pismen & Nir (1982) (apart from an erroneous minus sign, see Ngan & Dussan V., 1984), Hocking & Rivers (1982) and Cox (1986).

The general solution of [2.25] may be written

$$P(\varphi) = C a \ln x + \text{const}, \quad [2.26]$$

where

$$P(\varphi) = \int \frac{1}{A(\varphi)} d\varphi. \quad [2.27]$$

A series solution is obtainable for $P(\varphi)$ (Bronshtein & Semendyayev 1973):

$$P(\varphi) = \frac{(\varphi - \sin \varphi)}{2} + \frac{\varphi}{2} \left[\ln \frac{\tan(\varphi/2)}{\varphi/2} \right] - \sum_{n=1}^{\infty} 2^{2n} \frac{(2^{2n-1} - 1)}{(2n+1)!n} B_n \left(\frac{\varphi}{2}\right)^{2n+1}, \quad [2.28]$$

where B_n denotes the Bernoulli number,

$$B_n = \frac{2n!}{2^{2n-1} \pi^{2n}} \sum_{k=1}^{\infty} k^{-2n} \quad [2.29]$$

($B_1 = 1/6$, $B_2 = 1/30$, $B_3 = 1/42$, ...). The region of convergence of [2.28] is $[0, \pi]$.

It is worth noting that useful approximations to the functions $A(\varphi)$ and $P(\varphi)$ are provided by their small- φ limits

$$A(\varphi) \rightarrow 3/\varphi^2, \quad P(\varphi) \rightarrow \varphi^3/9; \quad \text{if } \varphi \rightarrow 0. \quad [2.30]$$

As table 2.1 shows these approximations are in practice good ones up to φ -values of about 150°

φ	$\varphi^2 A(\varphi)/3$	$9P(\varphi)/\varphi^3$
0	1	1
$\pi/4$	1.02	0.99
$\pi/2$	1.05	0.97
$3\pi/4$	0.92	0.99
$5\pi/6$	0.75	1.05
$11\pi/12$	0.46	1.20
π	0	∞

Table 2.1: accuracy of approximations [2.30]

Regime of validity

An indication of the error in the above, small-Ca solution for the meniscus shape is provided by the departure from unity, ϵ , of the ratio of the left- and right-hand members of [2.7], if [2.25] is inserted for $d\varphi/dx$:

$$\epsilon = \frac{1}{A(\varphi)\sin\varphi} \cdot \frac{d}{dx} (\sin\varphi \frac{d\varphi}{dx}) / (-\frac{Ca}{x^2}) - 1 \quad [2.31]$$

$$= \frac{-x^2}{\sin\varphi A(\varphi)} \cdot \frac{d}{dx} \left[\frac{\sin\varphi A(\varphi)}{x} \right] - 1 \quad [2.32]$$

$$= \frac{-x}{\sin\varphi A(\varphi)} \cdot \frac{d [\sin\varphi A(\varphi)]}{d\varphi} \cdot \frac{d\varphi}{dx} \quad [2.33]$$

$$= \frac{-Ca}{\sin\varphi} \cdot \frac{d [\sin\varphi A(\varphi)]}{d\varphi},$$

which, making use of [2.3], may be written

$$\epsilon = CaE(\varphi), \quad [2.34]$$

where

$$E(\varphi) = A(\varphi) [A(\varphi) \sin\varphi - 2 \cot\varphi]. \quad [2.35]$$

Evidently the small-Ca solution should provide a good approximation provided

$$Ca E(\varphi) \ll 1. \quad [2.36]$$

The large- φ limit

The function $E(\varphi)$ possesses simple small- and large- φ limits (table 2.2):

$$E(\varphi) \rightarrow 3/\varphi^3, \quad \varphi \rightarrow 0 \quad [2.37]$$

$$E(\varphi) \rightarrow 4/\pi, \quad \varphi \rightarrow \pi \quad [2.38]$$

φ	$E(\varphi)$	$\varphi^3 E(\varphi)/3$	$\pi E(\varphi)/4$
0	∞	1	∞
$\pi/4$	7.45	1.203	5.85
$\pi/2$	1.621	2.094	1.273
$3\pi/4$	1.164	5.075	0.914
π	1.273	13.16	1

Table 2.2: applicability of approximations [2.37] and [2.38]

For large φ , $E(\varphi)$ is constant and, consequently, also ϵ . This provides the clue to a large- φ solution of [2.7], of the same form as [2.26] but with Ca replaced by a function of itself, Ca' (see [2.31]):

$$P(\varphi) = Ca' \ln x + \text{const.} \quad [2.39]$$

The function Ca' is found by inserting the differential form of [2.39],

$$\frac{d\varphi}{dx} = \frac{Ca' A(\varphi)}{x}, \quad [2.40]$$

into [2.7]. The result is

$$Ca' \left[-1 + Ca' \frac{1}{\sin \varphi} \frac{d}{d\varphi} [A(\varphi) \sin \varphi] \right] = -Ca \quad [2.41]$$

or

$$Ca' [-1 - Ca' E(\varphi)] = -Ca. \quad [2.42]$$

For large φ , [2.42] is

$$Ca' = (\pi/8) [-1 \pm (1 + 16 Ca/\pi)^{\frac{1}{2}}]. \quad [2.43]$$

Since

$$Ca' \rightarrow Ca, \text{ if } Ca \rightarrow 0, \quad [2.44]$$

the positive root applies:

$$Ca' = (\pi/8) [(1 + 16 Ca/\pi)^{\frac{1}{2}} - 1]. \quad [2.45]$$

General approximation

As discussed earlier, [2.39] covers both the large- φ and small- Ca limits (in the latter case $Ca' \rightarrow Ca$ and, consequently, [2.39] \rightarrow [2.26] and is a candidate for a generally applicable solution to [2.7] in the wall region. Application of the boundary condition [2.16b] yields the final form of the equation:

$$P(\varphi) - P(\varphi_0) = Ca' \ln(x/\lambda). \quad [2.46]$$

Comparison with the exact solutions of the meniscus equation

To indicate the accuracy of approximation [2.46], a number of comparisons with numerical solutions of [2.7] and [2.13] are presented in the axi-symmetric case.

In figure 2.8 the model is compared with four numerical solutions (where $\xi_c = 5, 10, 15$ and 20) for moderate values of Ca and φ_0 , $Ca = 0.1$ and $\varphi_0 = 45^\circ$. In the wall

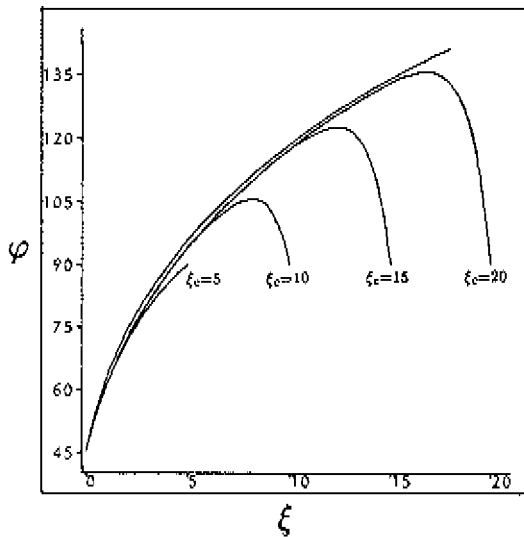


Fig 2.8 Comparison of the analytical approximation of the meniscus equation [2.18] with the exact solution for $\xi_c = 5, 10, 15$ and 20 ($Ca = 10^{-1}$, $\varphi_0 = 45^\circ$). The analytical approximation is the uppermost curve.

region the model describes the meniscus shape within about 2° . The effect of higher or lower Ca -values is examined in figures 2.9 and 2.10 ($Ca = 1$ and $Ca = 10^{-2}$, respectively). If anything, the agreement is better. Finally, larger and smaller φ_0 -values are examined in figures 2.11 and 2.12 ($\varphi_0 = 0^\circ$ and $\varphi_0 = 90^\circ$ respectively). For $\varphi_0 = 0^\circ$ the agreement is only to within about 7° , but for $\varphi_0 = 90^\circ$ the differences are minimal.

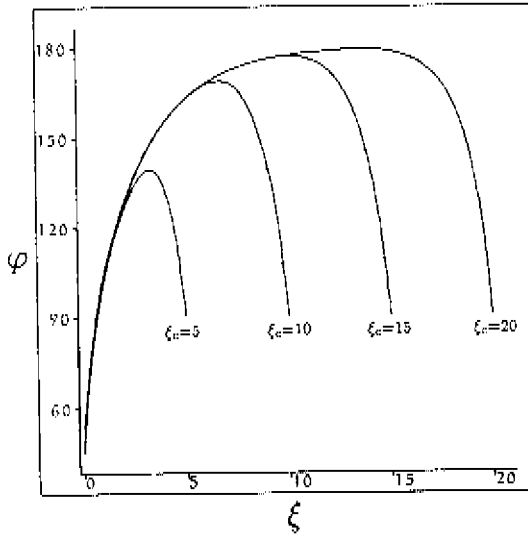


fig 2.9 Comparison of the analytical approximation of the meniscus equation [2.13] with the exact solution for $\xi_c = 5, 10, 15$ and 20 ($Ca = 1, \varphi_0 = 45^\circ$). In the wall region the analytical approximation is indistinguishable from the exact solutions.

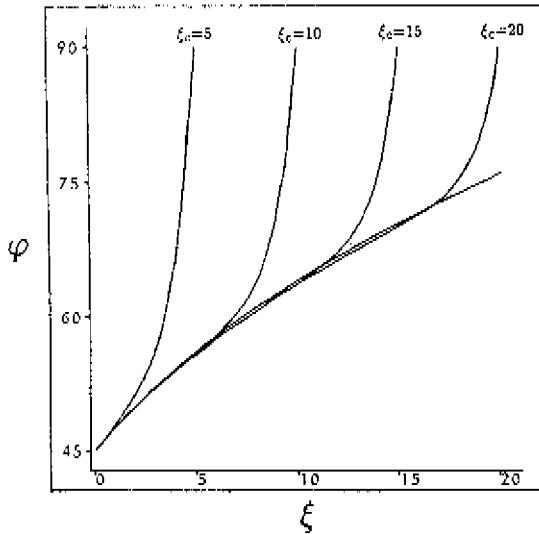


fig 2.10 Comparison of the analytical approximation of the meniscus equation [2.13] with the exact solution for $\xi_c = 5, 10, 15$ and 20 ($Ca = 10^{-2}, \varphi_0 = 45^\circ$).

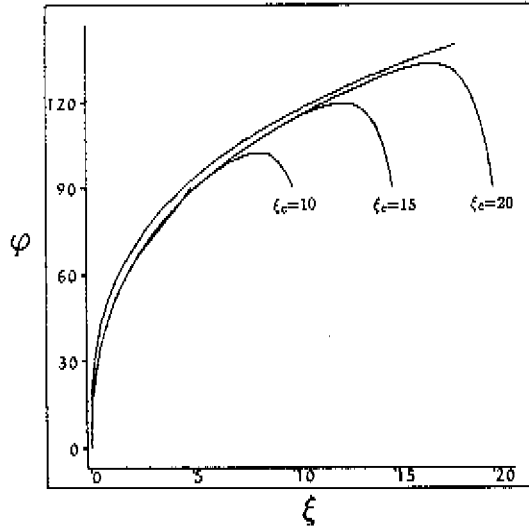


fig 2.11 Comparison of the analytical approximation of the meniscus equation [2.13] with the exact solution for $\xi_c = 5, 10, 15$ and 20 ($Ca = 10^{-1}$, $\varphi_0 = 0^0$).

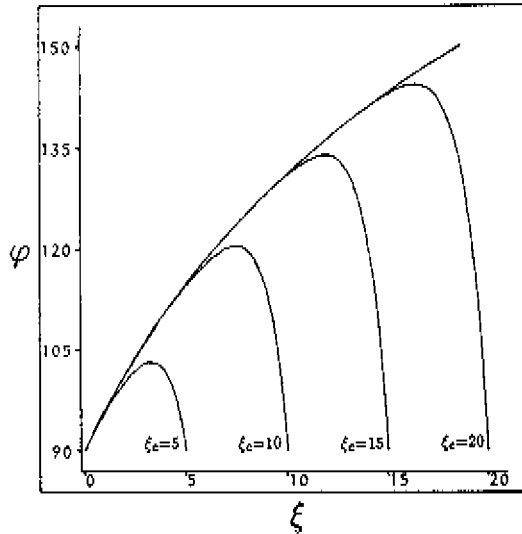


fig 2.12 Comparison of the analytical approximation of the meniscus equation [2.13] with the exact solution for $\xi_c = 5, 10, 15$ and 20 ($Ca = 10^{-1}$, $\varphi_0 = 90^0$).

2.8 Analytical approximation for the entire meniscus

The central region

In the central region of the meniscus the viscous stresses are of order $\mu U/a$, while the pressure difference between the liquid and gas is of order σ/a . Provided the ratio of these terms, Ca , is small, the central portion of the meniscus should have a very nearly spherical profile. The observations of Hoffman (1975) for capillary tubes confirm this expectation, surprisingly even for $Ca > 1$. The explanation of the latter fact probably lies in the viscous (deviatoric) contribution to the stress at the free surface which is negligible in the wall region (section 2.2) but not at the tube axis. This additional contribution will offset that due to pressure variation. Whatever the explanation, however, the result is useful and the next task consists of matching this central, circular profile to the wall solution [2.46].

Matching of the wall and central region

If, consistent with the preceding considerations, viscous normal stresses are neglected in the central region, the meniscus equation for the entire region may be written as

$$-\sigma\left(\frac{1}{R_1} + \frac{1}{R_2}\right) = p_v + p_c, \quad (2.47)$$

where p_c denotes the constant pressure in the central region and p_v the additional pressure due to viscous stresses. In the central region the term p_v may be neglected, while in the wall region this term dominates and R_2^{-1} and p_c may be neglected. In the transition region all terms are clearly significant.

The simplest matching procedure is to ignore the transition region and treat the central and wall approximations as valid up to some transition value of x , x_t . The optimal

choice of the transition point is clearly that at which the errors in the respective approximations are equal, that is where

$$|p_c + \sigma/R_2| = |p_v| . \quad [2.48]$$

For the tube geometry, R_2^{-1} is given at x_t by $\cos \varphi_t/(a-x_t)$. Consequently, $p_c = -2\sigma \cos \varphi_t/(a-x_t)$ and

$$|p_c + \sigma/R_2| = |\sigma \cos \varphi_t/(a-x_t)| . \quad [2.49]$$

Equation [2.49] also applies to the parallel-plate system since then $R_2 = \infty$ and

$p_c = -\sigma \cos \varphi_t/(a-x_t)$. An expression for p_v is obtained from the relations for the wall solution, [2.6] and [2.40]:

$$-p_v = \sigma \sin \varphi_t \text{Ca}' A(\varphi)/x_t . \quad [2.50]$$

Making use of [2.49] and [2.50], [2.48] yields the transition criterion:

$$\frac{x_t}{a} = \frac{\text{Ca}' A(\varphi_t) |\tan \varphi_t|}{1 + \text{Ca}' A(\varphi_t) |\tan \varphi_t|} . \quad [2.51]$$

Substitution of [2.51] into the solution for the wall region, [2.46], gives

$$P(\varphi_t) = P(\varphi_0) + \text{Ca}' \ln \left[\frac{a \text{Ca}' A(\varphi_t) |\tan \varphi_t|}{\lambda \cdot 1 + \text{Ca}' A(\varphi_t) |\tan \varphi_t|} \right] . \quad [2.52]$$

Given φ_0 , [2.52] can be solved iteratively to obtain φ_t and hence, via [2.51], x_t .

The dynamic contact angle

Defining the dynamic (apparent) contact angle φ_d as the angle obtained by extrapolating the circular profile in the external region to the wall, φ_d is obtained from φ_t and x_t by means of the relation

$$\cos \varphi_d = \cos \varphi_t / (1 - x_t/a) . \quad [2.53]$$

Consistent with the definition of φ_d in the analytical case, in the numerical case φ_d was taken as the angle obtained if the curvature at the tube axis were to persist up to the wall:

$$\varphi_d = \arctan \left[\left(\frac{1}{\eta c^2} - 1 \right)^{1/2} \right] , \quad [2.54]$$

for $\eta_c > 0$; and

$$\varphi_d = 180^\circ - \arctan\left[\left(\frac{1}{\eta_c^2} - 1\right)^{1/2}\right], \quad [2.55]$$

for $\eta_c < 0$.

2.9 Comparison with experimental results

The required boundary conditions at the wall

A comparison of the models developed above with measurements of φ_d is clearly possible only if values of φ_0 and λ can be specified. Ideally λ should be assigned a value larger than the range of intermolecular forces ($\approx 10^2$ nm) but much smaller than the system length scale, a . As pointed out by Kafka & Dussan V. (1979), the corresponding value of φ_0 should then be a material property in the sense that it depends only on the line speed for the given media. No data on such functional dependence of this value of φ_0 on U exist, however, and some plausible alternative must therefore be sought.

The simplest model, adopted here, is to suppose that the various classical approximations – the continuum and no-slip approximations and the idealization of a surface tension – retain their validity down to a distance from the wall of the order of a molecular dimension, at which point the true contact angle is attained (this concept having no meaning at submolecular distances). One result of this incorporation of the molecular nature of the liquid is that the much discussed stress singularity at the contact line does not arise. As discussed earlier, other authors have avoided this singularity by retaining the continuum approximation and assuming the no-slip approximation to lose its validity close to the contact line. However, the "slip length" required to obtain agreement with observed values of φ_d then proves to be of the order of a molecular dimension (Lowndes, 1980), which both undermines the credibility of the continuum treatment and points to a molecular explanation. This approach has also been followed by Voinov (1976, 1978).

To complete the boundary conditions at the wall, the true contact angle there is assumed to be sufficiently approximated by the static value

$$\varphi_0 = \varphi_s . \quad [2.56]$$

This assumption has been made by most authors, though Hoffman (1983) has presented arguments for substantial Ca -dependence of the true contact angle. At the large values of Ca at which the difference between φ_0 and φ_s is likely to become appreciable, however, the value of φ_d predicted by [2.51]–[2.53] depends only weakly on φ_0 . Numerically obtained results of φ_d versus φ_0 for a few Ca -values are shown in figure 2.13 for $\xi_c=14$. The validity

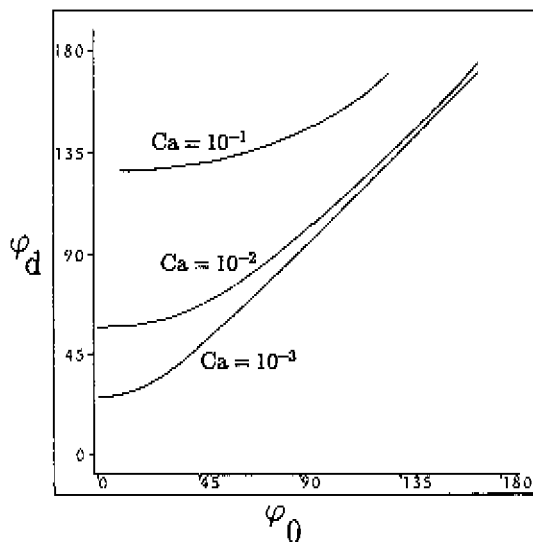


fig 2.13 *The dependence of the dynamic contact angle on the true contact angle at the wall for various Ca ($\xi_c = 14$).*

of approximation [2.56] is thus less crucial to the prediction of φ_d than it would at first sight appear. (Conversely, good agreement between observations and predictions based on the approximation [2.56] furnishes no proof of the accuracy of this approximation!)

Comparisons

The values of the dynamic contact angle predicted by the analytical approximation [2.51] – [2.53] and those obtained by numerical solution of the meniscus equation [2.13] can now be compared with those found experimentally in tubes [Hoffman (1975) and corroborated by Fermigier & Jenffer (1988)].

The resulting comparisons are set out in figures 2.14–2.17 for a λ -value of 1 nm. While the best-fit value of this length scale cannot be specified to better than a factor of 5 or so, it is certainly of the order of a molecular dimension.

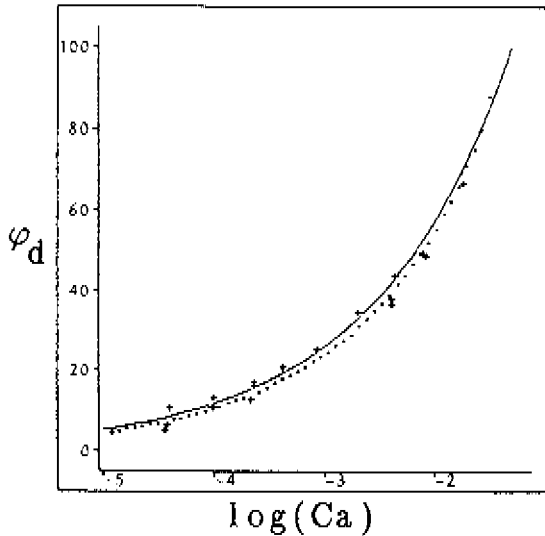


Fig. 2.14 *Ca*-dependence of the dynamic contact angle as measured by Hoffman (+), as predicted by the analytical approximation equations [2.51]–[2.53] (· · ·) and as predicted by the meniscus equation [2.13] (—). The liquid used in Hoffman's experiments was G.E. Silicone Fluid SF-96 ($\mu = 0.958$ kg m⁻¹ s⁻¹, $\sigma = 2.18 \cdot 10^{-2}$ N m⁻¹, static contact angle = 0°).

At $Ca < 10^{-1}$, both models are seen to agree well with the experimental results. For larger Ca , the analytical approximation continues to provide an excellent prediction while,

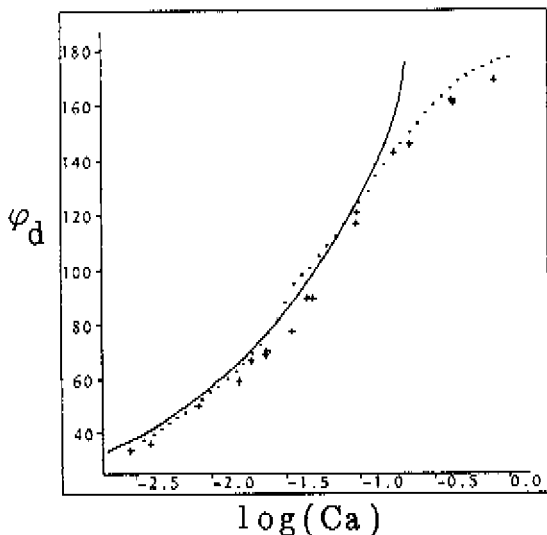


Fig. 2.15

Ca -dependence of the dynamic contact angle as measured by Hoffman (+), as predicted by the analytical approximation equations [2.51]–[2.53] (· · ·) and as predicted by the meniscus equation [2.19] (—). The liquid used in Hoffman's experiments was Brookfield Std. Viscosity Fluid ($\mu = 98.8 \text{ kg m}^{-1} \text{ s}^{-1}$, $\sigma = 2.17 \cdot 10^{-2} \text{ N m}^{-1}$, static contact angle = 0°).

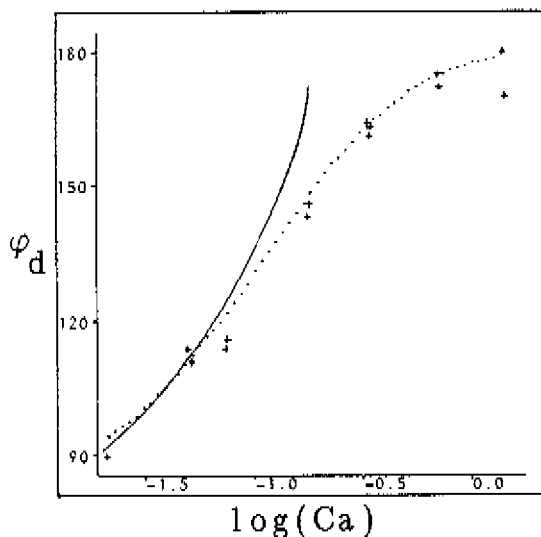


Fig. 2.16

Ca -dependence of the dynamic contact angle as measured by Hoffman (+), as predicted by the analytical approximation equations [2.51]–[2.53] (· · ·) and as predicted by the meniscus equation [2.19] (—). The liquid used in Hoffman's experiments was Ashland Chem. Admex 760 ($\mu = 109.9 \text{ kg m}^{-1} \text{ s}^{-1}$, $\sigma = 4.98 \cdot 10^{-2} \text{ N m}^{-1}$, static contact angle = 69°).

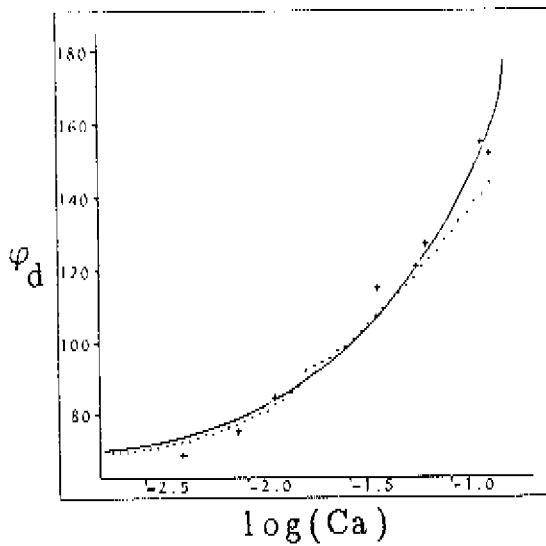


Fig. 2.17

Ca-dependence of the dynamic contact angle as measured by Hoffman (+), as predicted by the analytical approximation equations [2.51]–[2.53] (---) and as predicted by the meniscus equation [2.13] (—). The liquid used in Hoffman's experiments was Santicizer 405 ($\mu = 11.2 \text{ kg m}^{-1} \text{ s}^{-1}$, $\sigma = 4.94 \cdot 10^{-2} \text{ N m}^{-1}$, static contact angle = 67°).

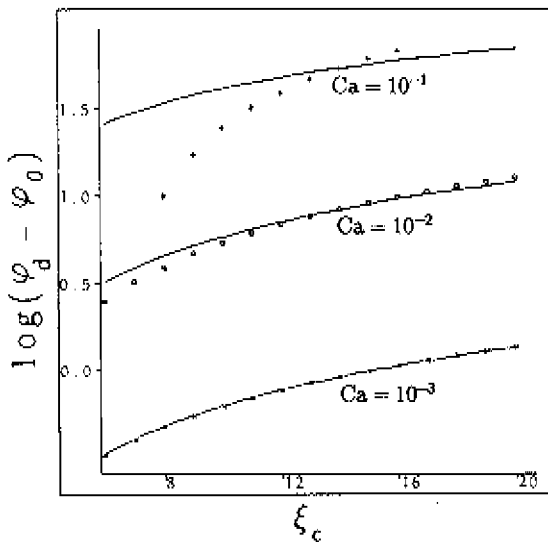


Fig. 2.18

The dependence of the dynamic contact angle on the system scale (represented by ξ_c) as predicted by meniscus equation [2.13] (—) and by Kafka & Dussan V. (symbols), for various *Ca* and $\phi_0 = 90^\circ$. At $\xi_c = 14$ both models are made to agree.

paradoxically, the model based on the neglect of fewer terms fails. On reflection this result is understandable. Both models are reliable in the wall region. In the central region, however, the analytical approximation assumes a circular profile which, as discussed in section 2.8, somewhat fortuitously proves to be a better approximation than that obtained taking account of pressure variation but neglecting viscous normal stresses.

2.10 System-dependence of the dynamic contact angle

The minor influence of system geometry on meniscus shape (and, by implication, on dynamic contact angle) has been illustrated in figure 2.5. The effect of system scale, a , is reflected, for a given geometry, in the influence of ξ_c ($=\ln(a/\lambda)$). Figure 2.18 illustrates the fact that the dependence of the dynamic contact angle on the system scale is similarly weak. The case $\varphi_0 = 90^\circ$ has been chosen to allow a comparison with the small-Ca prediction of Kafka & Dussan V. (1979).

The figure equally demonstrates the weak dependence, for a given system, of the dynamic contact angle on the length scale λ .

2.11 Conclusions and final discussion

An alternative to full numerical solution of the flow and meniscus shape associated with an advancing liquid-gas contact line has been explored, based on a local-wedge approximation. Up to $Ca \approx 10^{-1}$ the associated errors are acceptable over the entire meniscus, as supported by the excellent agreement with available numerical solutions. At higher Ca, for which viscous stresses become significant in the central region of the meniscus, only the wall region is adequately described by the approximation. Good agreement with measured values of the advancing contact angle is nevertheless obtained if the wall profile is matched to a circular central profile. This leads to an analytical

approximation for the dynamic contact angle, applicable at all Ca .

Since the local-wedge approximation involves no assumption as to the sign of the line speed it should be applicable in the liquid-gas *receding* case and can probably be extended to the liquid-liquid case also (which involves both advancing and receding liquids). Indeed, as will be shown in next chapter, in these cases Ca -values are likely to be limited to order 10^{-1} or less, a film of the receding liquid being left behind at larger Ca .

The question of the appropriate boundary conditions at the solid surface remains unsettled, the only contribution of the present chapter being to demonstrate that boundary conditions taking account of the discontinuous nature of the liquid but retaining the no-slip approximation are as successful in removing the wall singularity and in predicting the dynamic contact angle as are the reverse assumptions. However, neither these assumptions nor that of constant true contact angle are severely tested in the advancing case, the predicted dynamic angle being relatively insensitive to conditions at the wall. It is noteworthy that this will not be so if the liquid is receding and comparison of predictions and experiment in this case should be highly illuminating.

Finally, let it be noted that the model developed predicts a weak system-dependence of the dynamic contact angle (for example tube-radius dependence: [2.51]–[2.53]) which cannot, as noted by Kafka & Dussan V. (1979), be viewed as a material property.

CHAPTER 3 – *An approximate solution of the hydrodynamic problem associated with receding liquid–gas contact lines*

3.1 Introduction

While advancing liquid–gas contact lines have been the subject of attention for some time, most research into receding lines is relatively recent. The most striking feature of receding contact lines, in contrast with advancing contact lines, is the existence of a maximum speed of dewetting as demonstrated experimentally by Blake & Ruschak (1979). For small capillary numbers, Ca , a hydrodynamic description was given by Voinov (1976, 1978), de Gennes (1986), Cox (1986) and Teletzke, Davis & Scriven (1988), the latter incorporating not only hydrodynamics but also disjoining pressure. Spontaneous dewetting of a parallel film on plane surfaces has been described by Brochard, Redon & Rondelez (1988), Brochard–Wyart & Dailant (1990), Redon, Brochard–Wyart & Rondelez (1991) and of film on fibres by Brochard–Wyart, Meglio & Quéré (1987). A few experimental studies examined the receding contact line by withdrawing a polyester tape [Petrov & Sedev (1985)] or a glass rod [Sedev & Petrov (1988/89), Sedev & Petrov (1991)] from a liquid. Receding contact lines with surfactants were studied by Petrov & Radoev (1981), de Gennes (1986) and Hopf & Geidel (1987). Receding contact lines in the geometry of a capillary have not been the subject of a large number of studies. Rillaerts & Joos (1980) examined experimentally almost exclusively advancing contact angles in a tube. They reported that "the receding contact angle became rapidly zero". One study of Quéré (1991) examined experimentally the relation between the static contact angle and the capillary number at which a film starts being left behind, the critical capillary number.

In this chapter the simplified approach to the hydrodynamics of moving contact

lines, developed in chapter 2 in the context of advancing lines without restriction on the magnitude of Ca , is applied to the problem of a steadily receding liquid-gas contact line. The approach supposes the system length scale to be sufficiently small and the liquid sufficiently viscous for gravitational and inertial stresses, aside from a uniform pressure, to be negligible in the gas.

Like other analyses of the line-speed dependence of the apparent (or "dynamic") contact angle, the region adjoining the line is split into a region in which the classical concepts of surface tension and the continuum approximation apply and a region very close to the line in which one or more of these concepts breaks down. In the former region, the approach developed in chapter 2 reduces the free-surface hydrodynamic problem concerned to a second-order ordinary differential equation for the variation of meniscus inclination with distance from the wall by making use of the fact that this variation is typically slow in an appropriate dimensionless sense, so that analytical solutions for the flow and pressure variation in a plane wedge are applicable locally. The existence of the non-classical region was incorporated in chapter 2 by including the only feature known with certainty — that the continuum description, and with it concepts such as the meniscus inclination, loses its validity at a distance from the wall minimally of the order of a molecular dimension. The meniscus inclination at this distance from the wall, the true contact angle, was furthermore for simplicity's sake supposed to be adequately approximated by the equilibrium (static) value¹. The latter assumption was not, however, severely tested by the ensuing comparison of predicted and measured dynamic angles since for the large line speeds at which an appreciable deviation from the static angle might be expected the dynamic angle proves relatively insensitive to the value of the true angle.

The meniscus equation derived in chapter 2 contains no assumption as to the sign of

¹The solid is supposed to be perfectly smooth and chemically homogeneous, resulting in equal advancing and receding static angles. In reality a certain hysteresis is always present (see section 3.7).

the line speed and is consequently applicable to receding liquid-gas contact lines as well.

3.2 The differential equations describing receding menisci

With respect to a reference frame moving with the contact line, a receding meniscus may be described by means of the coordinates x and φ (figure 3.1, φ in radians). Neglecting

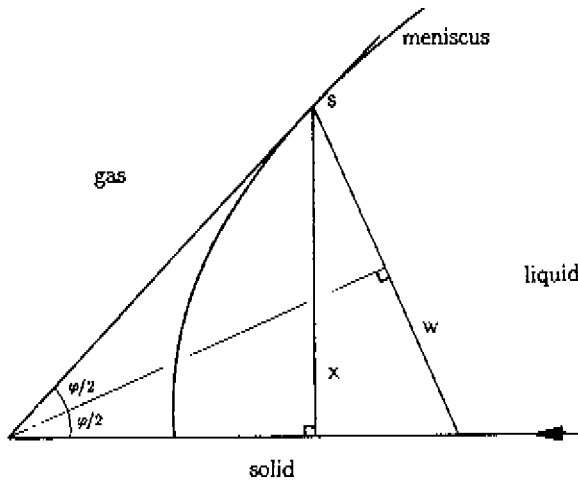


Fig 3.1 Definition of variables for a receding meniscus.

gravitational and inertial forces, the differential equation describing an *advancing* meniscus between two parallel planes, when a viscous liquid replaces a gas over a smooth homogeneous surface, is shown in chapter 2 to be

$$\frac{1}{A(\varphi)} \frac{d}{d\varphi} \left(\sin \varphi \frac{d\varphi}{dx} \right) = \frac{-Ca}{x^2}, \quad [3.1]$$

where

$$A(\varphi) = \frac{-2 \sin \varphi}{\sin \varphi \cos \varphi - \varphi} \quad [3.2]$$

and

$$Ca = \frac{\mu U}{\sigma} \quad [3.3]$$

is the dimensionless line speed, or capillary number (μ, U and σ are the viscosity of the

advancing fluid, the speed of the contact line and the surface tension respectively). As noted above, equation [3.1] is based on a local-wedge approximation for the flow and pressure gradient which should be acceptable provided that angle φ varies slowly in a dimensionless sense:

$$\frac{d\varphi/\varphi}{ds/w} \ll 1 \quad [3.4]$$

(s and w are the arc length along the meniscus and the local wedge width respectively: figure 3.1).

The derivation of [3.1] places no restriction on the sign of the line speed and [3.1] thus also applies to a receding meniscus ($Ca < 0$), provided [3.4] is satisfied. (With $U < 0$, μ becomes the viscosity of the receding fluid.)

Likewise the differential equation describing an advancing meniscus in a tube

$$\frac{d}{dx} \left(\sin \varphi \frac{d\varphi}{dx} + \frac{\cos \varphi}{a-x} \right) = \frac{-Ca}{x^2} \frac{A(\varphi) \sin \varphi}{x} \quad [3.5]$$

(in which a is the tube radius), derived in chapter 2, should be applicable to the receding case also.

The boundary conditions to be satisfied by [3.1] or [3.5] at the wall are again taken to be

$$\varphi = \varphi_0, \text{ at } x = \lambda, \quad [3.6]$$

where λ is a distance minimally of the order of a molecular dimension and φ_0 the true contact angle. Alternatively, λ and φ_0 may be viewed as phenomenological parameters whose magnitude must be determined from experiment and whose interpretation must await more detailed consideration of the region adjoining the line. As discussed in the advancing case, there is no a priori justification for the assumption that φ_0 remains equal to the static contact angle, φ_s . Furthermore, in contrast with the advancing case, any variation of φ_0 with line speed proves of major influence on the apparent or "dynamic" contact angle, φ_d , in the receding case.

In chapter 2 the dynamic contact angle is defined as the angle obtained if the central, circular profile of the meniscus is extrapolated to the wall. In the receding case a

closely circular central profile is often absent and a more practical definition is the angle which a circular/spherical meniscus having the same apex height h as the actual meniscus makes with the wall (figure 3.2):

$$\varphi_d = \cos^{-1}\left(\frac{2ha}{a^2+h^2}\right) . \quad [3.7]$$

In cases in which a large spherical portion exists the two definitions of φ_d become equivalent.

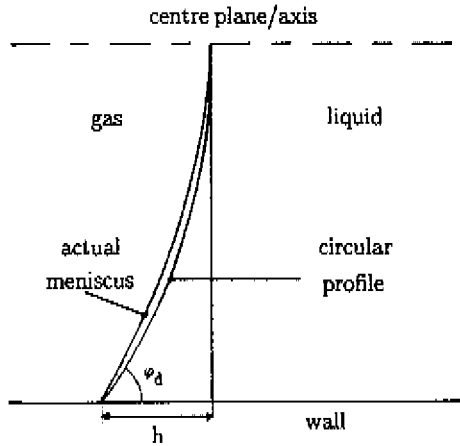


Fig 3.2 Definition of the dynamic contact angle, φ_d .

3.3 Solution of the meniscus equation

The differential equations [3.1] and [3.5] are solved as indicated in chapter 2, making use of a logarithmic scale of distance

$$\xi = \ln(x/\lambda) , \quad [3.8]$$

by numerically integrating from the centre line/centre axis ξ_c to the distance λ from the wall ($\xi=0$) using a second-order finite-difference scheme. The subscript c is used to identify a property on the centre plane/centre axis and the subscript 0 a property at $\xi=0$. The integration procedure requires the values of φ_c and η_c where

$$\eta = \frac{d\varphi}{d\xi} \quad [3.9]$$

Symmetry requires that φ_c be 90° . The value of η_c determines the value of φ_0 obtained.

To investigate the effect of system configuration on the shape of the receding menisci, menisci are examined between plates and in a tube for the case $\varphi_0 = 138.15^\circ$, $\xi_c = 15^2$ and $Ca = -0.1$ (roughly the largest value of $|Ca|$ for which a solution exists, as will be clear later). In the tube case the corresponding values of η_c and φ_d are 0.77 and 53° while the corresponding values in the parallel-plate case are 1.00 and 41° . Although this difference appears considerable the capillary number required in the tube case to obtain $\eta_c = 1$ (with $\varphi_0 = 138.15^\circ$ and $\xi_c = 15$) is in fact only marginally larger: -0.102 . For smaller capillary numbers this difference becomes even smaller, vanishing completely for $Ca=0$. Only the tube case will be further examined in detail in this chapter.

The meniscus equation [3.5] is solved for different η_c values. In figure 3.3 φ_0 is given as a function of η_c (where $\xi_c=15$ and $Ca=-0.1$). In contrast with the situation for positive capillary numbers, φ_0 is *not* a monotonic function of η_c but exhibits a minimum ($\varphi_{0,\min}=137.0^\circ$). Evidently for $\varphi_0 < \varphi_{0,\min}$ no solution of [3.5] exists while for $\varphi_0 > \varphi_{0,\min}$ there are two solutions. These two solutions for $\varphi_0=137.2^\circ$ are shown in figure 3.4 ($\eta_c=0.98$ for the upper curve and $\eta_c=1.30$ for the other one). For the solutions having $d\varphi_0/d\eta_c > 0$ (see figure 3.3) it is found that $d\eta_c/dCa > 0$ (for constant φ_0 and ξ_c) and consequently that $d\varphi_d/dCa < 0$, which is contrary to experimental findings (Dussan V., 1979). The solutions for which $d\varphi_0/d\eta_c > 0$ will therefore be ignored. These solutions are presumably unstable and in that case not encountered in reality.

In general $\varphi_{0,\min}$ is a function of the capillary number and of ξ_c . In figure 3.5 $\varphi_{0,\min}$

² The order of magnitude corresponding to tubes of order 1 mm, assuming λ to be of the order of 1 nm.

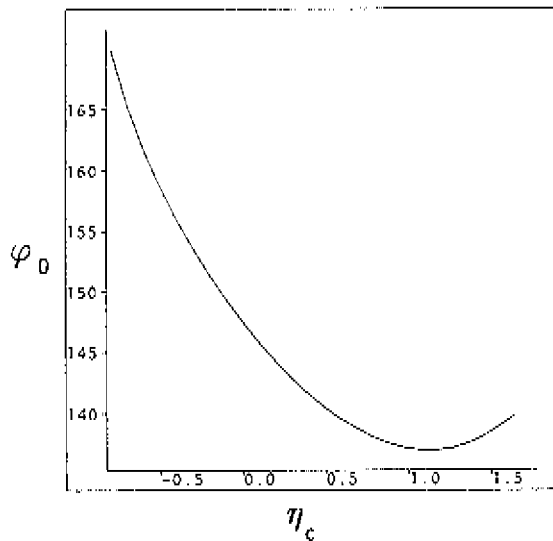


Fig 3.3 Variation of required value of the true contact angle, φ_0 , with central profile curvature, η_c : depending on the value of φ_0 , either no or two solutions exist ($Ca = -0.1$, $\xi_c = 15$).

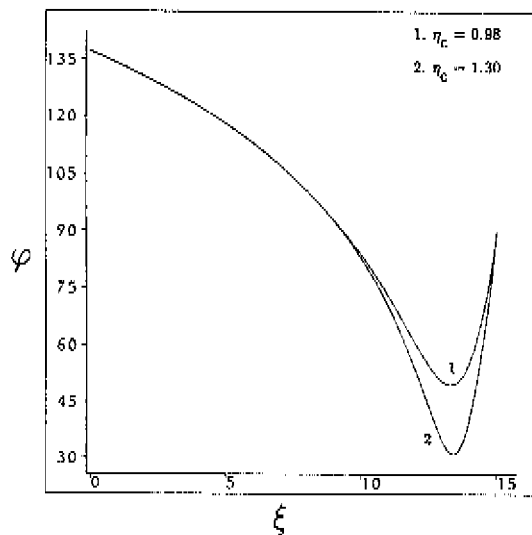


Fig 3.4 Meniscus profile for the two solutions ($Ca = -0.1$, $\xi_c = 15$, $\varphi_0 = 137.2^\circ$).

is given as a function of $\log(-Ca)$ for different ξ_c -values. In a given system there thus exists a capillary number (the critical capillary number) beyond which (in absolute value) there is no solution to the differential equation describing a stationary receding meniscus. Beyond the critical capillary number, unsteady effects are therefore to be expected, probably resulting in a film of liquid being left behind.

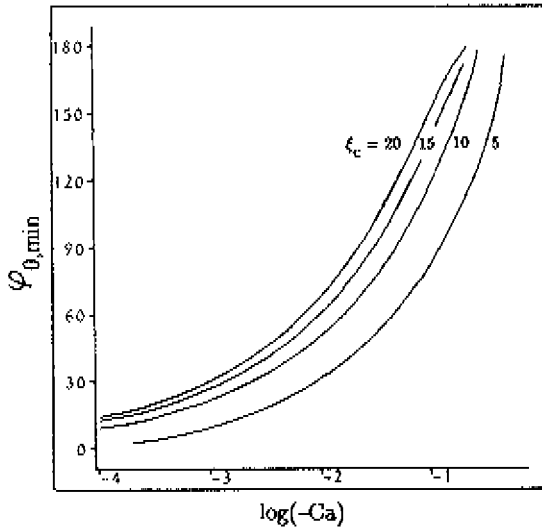


Fig 3.5 Variation of $\varphi_{0, \min}$ with the capillary number for various system scales. Equivalently, the figure indicates the dependence of the critical capillary number on the true contact angle, φ_0 .

3.4 Dynamic contact angles

In figure 3.6 φ_d is presented as a function of $\log(-Ca)$ for three values of ξ_c and of φ_0 . The authors know of no data on φ_0 as a function of the contact line speed. Should φ_0 remain constant (equal to φ_s) then the curves in figure 3.6 would represent the actual variation of φ_d in a given system. Conversely the actual variation of φ_d provides

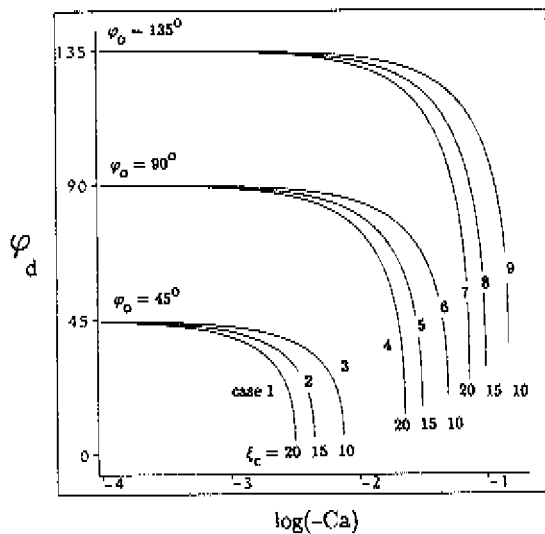


Fig 3.6 The dynamic contact angle presented as a function of the capillary number for various true contact angles and system scales (λ -values).

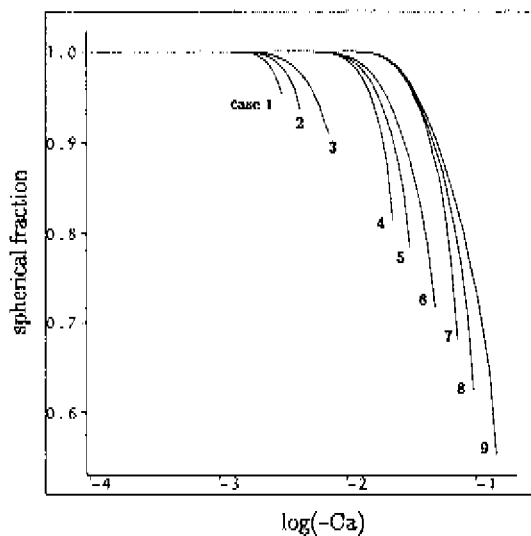


Fig 3.7 Spherical fraction of the meniscus for the cases studied in figure 3.6.

information on any U -dependence of φ_0 . More will be said on this subject in section 3.6.

As noted earlier, various authors have defined the dynamic contact angle (especially in experimental work) as the angle which the circular profile of a moving meniscus seems to make with the wall. This definition is equivalent to [3.7] only if the greater part of the meniscus profile is circular. To obtain an impression of the extent of the central, circular portion of the meniscus, the meniscus is here defined as circular if it deviates from the extrapolation of the circular profile at the tube axis by less than 3° (a not far-fetched uncertainty for measurements). The spherical fraction of the meniscus is given as a function of the capillary number in figure 3.7, defining this fraction as $(a-x_s)/a$, where x_s denotes the 3° -deviation point. Near the critical capillary number, the predicted deviations of the meniscus from the spherical shape should be detectable in experiments, especially for larger true contact angles.

3.5 The local-wedge approximation

In figure 3.8 the dimensionless wedge-angle variation rate, $(d\varphi/\varphi)/(ds/w)$ is examined for capillary numbers close to the critical. In the wall region where the deviation from the spherical becomes major, this parameter is maximally about 0.2 — a situation similar to that found in the advancing case for a capillary number of order 10^{-1} , where close agreement with both numerical and experimental results is found. As discussed in chapter 2, the requirement [3.4] is never satisfied in the central circular region, implying that the deviation from a circular profile predicted by [3.5] will not be accurate. Since this deviation is small, however, the total error remains acceptable. For smaller capillary numbers [3.4] is still better satisfied: figure 3.9.

There is thus good reason to expect that the solutions also provide a good approximation, the main uncertainty lying in the value of φ_0 , as discussed below.

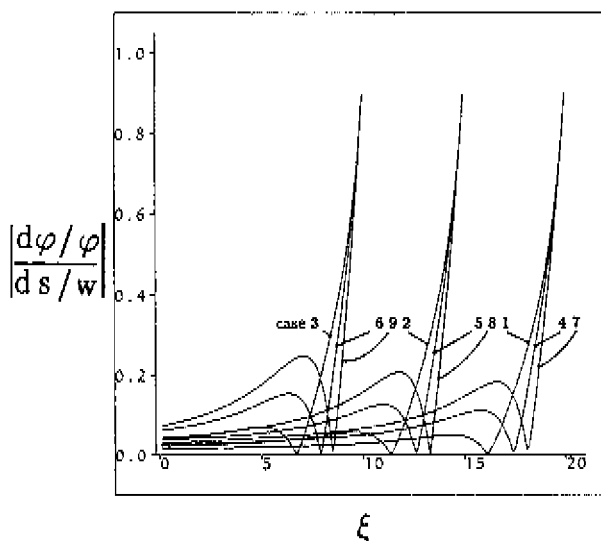


Fig 3.8 The dimensionless wedge-angle variation rate $\left| (d\varphi/\varphi)/(ds/w) \right|$ as a function of ξ for the cases studied in figure 3.6 ($\eta_c=1$, capillary number close to the critical value).

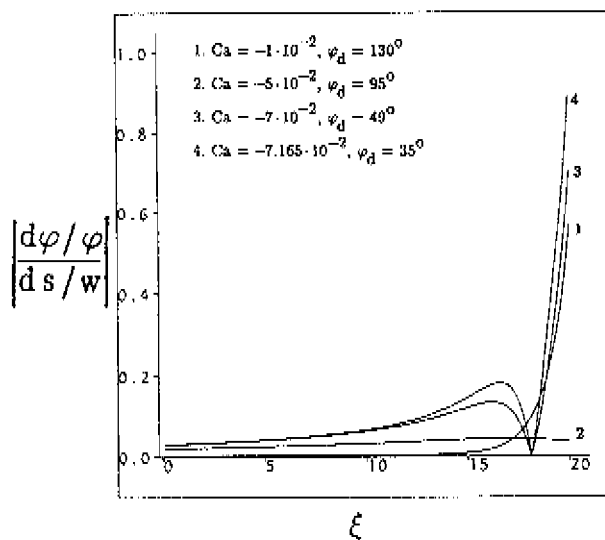


Fig 3.9 The dimensionless wedge-angle variation rate $\left| (d\varphi/\varphi)/(ds/w) \right|$ as a function of ξ for various capillary numbers ($\xi_c=20$, $\varphi_0=135^\circ$).

3.6 Dynamic contact angle dependence on system scale and true contact angle

In figure 3.10 the predicted dynamic contact angle dependence on the system scale a ($/\lambda$ -value, since $\xi_c = \ln(a/\lambda)$) is presented for $\varphi_0 = 135^\circ$ and various values of the capillary number. In contrast with the advancing case the dynamic contact angle is seen to depend strongly on ξ_c especially as the critical capillary number is approached.

In figure 3.11 the dynamic contact angle dependence on φ_0 is shown for $\xi_c = 15$ and various capillary numbers. Again in contrast with the advancing case, the dynamic contact angle is very sensitive to changes in φ_0 , this sensitivity once more increasing as the critical capillary number is approached.

In view of the strong φ_0 -dependence of φ_d , measurements of φ_d should provide an indication of the variation of the true contact angle with line speed. In next section a comparison of the predicted critical capillary number with recently obtained experimental values is undertaken.

3.7 Comparison with experimental results

Receding contact lines in a tube geometry have recently been experimentally investigated by Q  r   (1991). Drops of various alkanes were displaced inside a teflon capillary tube by applying a pressure difference over the drop and the capillary number was investigated at which the drop first leaves a film behind. Static contact angles for this system, deduced from microbalance measurements, exhibited considerable hysteresis, receding angles, φ_r , being around 20° less than advancing. Figure 3.12 compares the critical capillary numbers found by Q  r   for different values of φ_r with predictions of the present model assuming that

$$\varphi_0 = \varphi_r, \quad [3.10]$$

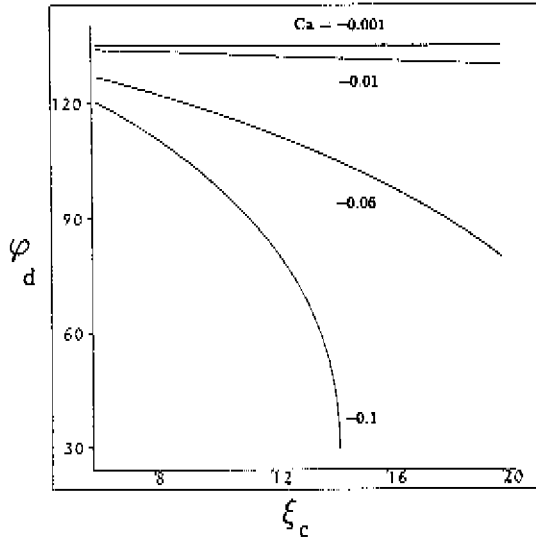


Fig 9.10 The dependence of the dynamic contact angle on the system scale (λ -value) for various capillary numbers ($\varphi_0=135^\circ$).

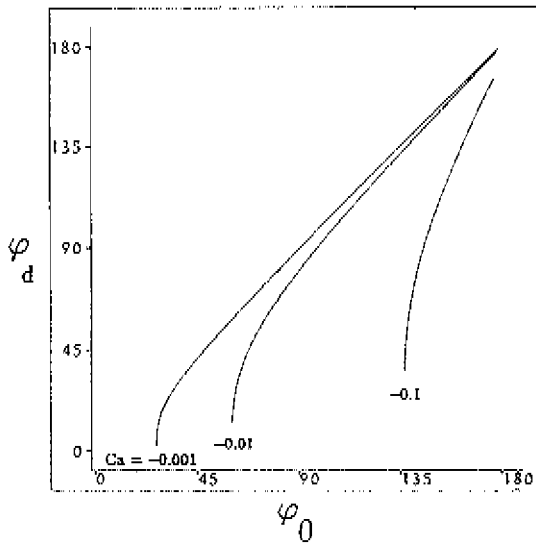


Fig 9.11 The dependence of the dynamic contact angle on the true contact angle at the wall for various capillary numbers ($\xi_c=15$).

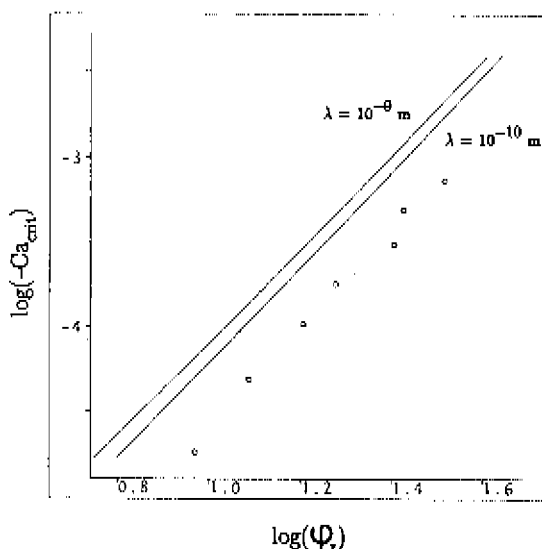


Fig 3.12 Comparison of the critical capillary numbers obtained experimentally by Quéré (points) with those predicted by the model (continuous lines) as a function of the (receding) static angle, assuming that $\varphi_0 = \varphi_r$ (φ_r in degrees).

or two values of λ : 10^{-9} and 10^{-10} m (the latter representing the lowest plausible value). While the order of magnitude and φ_r -dependence of Ca_{crit} are well predicted by the model, the values of Ca_{crit} appear³ to be overpredicted by a factor of 2 or more.

Various possible explanations of this discrepancy present themselves. It may be related to the non-ideal nature of the solid surface concerned (as indicated by the substantial hysteresis observed in the static angles). It may reflect inaccuracies in the local-wedge approximation, though the success of this approximation in the advancing case suggests this is unlikely. Alternatively it may be indicative of a deviation of the true contact angle from the static (receding) value at the capillary number concerned, good

³The error bounds indicated by Quéré on the lower φ_r -values are greater than the discrepancy concerned; for the larger φ_r -values, however, this is not the case.

agreement with the measurements being obtained for a λ -value of 10^{-9} m if it is supposed that

$$\varphi_0 = 0.68 \varphi_r . \quad [3.11]$$

The factor 0.68 would presumably increase as Ca decreases, becoming 1 in the static limit.

3.8 Final discussion

The present model, like others, predicts a maximum capillary number, Ca_{crit} , above which no stationary receding meniscus exists. Unlike other models, however, excepting that of de Gennes' (1986), the limiting value of the dynamic contact angle at Ca_{crit} is not predicted to be zero, except in the limit of small true contact angle, φ_0 . The portion of the meniscus which is significantly deformed from the spherical is furthermore predicted to be considerable unless φ_0 is small. The critical capillary number is predicted to exhibit a strong dependence on the system scale (λ -value) and the true contact angle. It is this strong dependence which enables conclusions to be drawn from experiments regarding the values of φ_0 or λ . The comparison of the predictions of the model with the experiments of Quéré suggests that at the critical capillary number the true contact angle is significantly smaller than the static angle by a factor which is seemingly independent of the static contact angle for the alkane-*teflon* system concerned. Measurements of the Ca-dependence of φ_d , would permit this factor to be evaluated for smaller Ca-values.

CHAPTER 4 – *An approximate solution of the hydrodynamic problem associated with moving liquid–liquid contact lines*

4.1 Introduction

While in the past advancing liquid–gas contact lines have been studied extensively, contact lines formed between two viscous liquids (liquid–liquid contact lines) have received attention only in recent years. For a review article on dynamic contact lines see for instance Dussan V. (1979) or de Gennes (1985).

When a viscous liquid advances over a smooth homogeneous solid displacing a gas of negligible viscosity, viscous forces have a strong influence on the meniscus shape, especially close to the wall. The meniscus profile has been studied using methods based on perturbation techniques: Hansen & Toong (1971b), Huh & Mason (1977), Greenspan (1978), Kafka & Dussan V. (1979), Neogi & Miller (1982), Hocking & Rivers (1982), Cox (1986), de Gennes, Hua & Levinson (1990), or using a direct numerical (finite–element) solution: Lowndes (1980). If the classical concepts of viscosity and surface tension are maintained up to the contact line a singularity arises at the contact line. This singularity is often removed by supposing the liquid to slip in a small region near the contact line. Various slip models have been used, the mutual differences having only a minor influence on the total meniscus shape. An alternative approach to the hydrodynamic problem concerned has been developed in chapter 2; this results in a second–order differential equation for the meniscus shape, based on a local–wedge approximation which is acceptable provided the meniscus inclination varies slowly with the distance from the wall. The singularity is avoided by taking account of the fact that at very small distances from the wall (of the order of molecular dimensions) the continuum concepts break down. At

this distance the meniscus inclination reaches its final value, the true contact angle. In recent years the breakdown of continuum hydrodynamics has become a more and more popular solution to the singularity problem. Thompson & Robbins (1989) showed in a molecular dynamics study that slip at the contact line appears to be associated with the breakdown of local hydrodynamics at molecular scales.

The approach to the hydrodynamic problem developed in chapter 2 has been used in chapter 3 to describe receding contact lines, where a gas of negligible viscosity displaces a viscous liquid over a smooth homogeneous surface. A maximum "critical" capillary number at which a stable meniscus exists was established. A maximum speed of dewetting was also found in other investigations, both experimental and theoretical.

The hydrodynamic problem associated with a moving liquid-liquid contact line involves both an advancing and a receding fluid. It has been studied for a plane-interface geometry by Huh & Scriven (1971); once more a singularity arises at the actual contact line. A theoretical description for small line speeds, based on a perturbation approach and involving a matched asymptotic expansions technique, was given by Cox (1986). Measurements of the shape of a moving meniscus between two viscous liquids in a capillary tube have been performed by Fermigier & Jenffer (1988). The dynamic contact angle has been measured in very fine capillaries by Legait & Sourieau (1985) by measuring the pressure difference over a moving meniscus. A finite-element solution of the hydrodynamic problem for a number of line speeds and true contact angles has been given by Tilton (1988) and a finite-difference solution by Zhou & Sheng (1990), the singularity being avoided by introducing slip. Zhou & Sheng compared their predictions with the experimental results of Fermigier & Jenffer and concluded that in some cases the true contact angle at the wall depends on the contact line speed.

The aim of this chapter is to apply the approach used in chapter 2 and 3 to describe advancing and receding contact lines to the case of liquid-liquid contact lines.

4.2 The equation governing a steadily moving meniscus between two viscous liquids

Plane geometry

The stream functions Ψ_R and Ψ_A of creeping liquid flows in two plane complementary wedges (one with wedge angle φ) with a constant velocity U prescribed on one boundary (figure 4.1) have been given by Huh and Scriven (1971) in polar coordinates

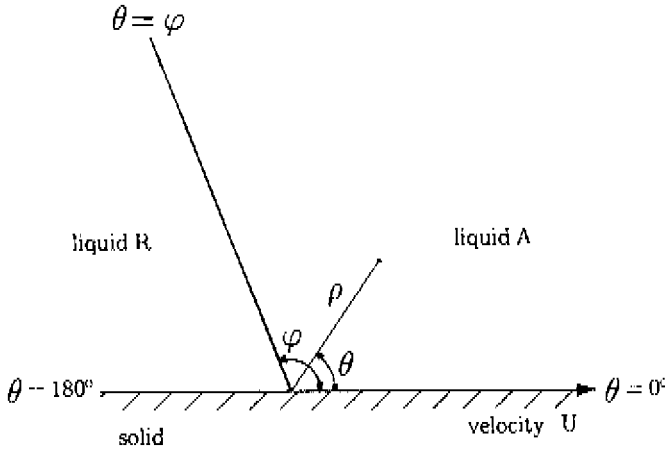


Fig 4.1 *Viscous flow in plane complementary wedges adjoining a moving solid boundary.*

ρ and θ as

$$\Psi_R(\rho, \theta) = U\rho(a_R \sin \theta + b_R \cos \theta + c_R \theta \sin \theta + d_R \theta \cos \theta) \quad [4.1]$$

and

$$\Psi_A(\rho, \theta) = U\rho(a_A \sin \theta + b_A \cos \theta + c_A \theta \sin \theta + d_A \theta \cos \theta) \quad [4.2]$$

For the coefficients a_R, \dots, d_A see appendix D (the subscripts R and A denoting receding and advancing). Using standard methods in fluid mechanics the pressures p in the liquids at the interface are found to vary (along the interface) as

$$\frac{\partial p_R}{\partial \rho} = U \frac{2\mu_R}{\rho^2} (c_R \sin \varphi + d_R \cos \varphi) \quad [4.3]$$

and

$$\frac{\partial p_A}{\partial \rho} = U \frac{2\mu_A}{\rho^2} (c_A \sin \varphi + d_A \cos \varphi) \quad [4.4]$$

where μ_R and μ_A are the respective liquid viscosities. The deviatoric component of the normal stress is zero. From [4.3] and [4.4], it follows that the pressure difference gradient at the interface is given by

$$\frac{\partial(p_R - p_A)}{\partial \rho} = U \frac{2\mu_R}{\rho^2} (c_R \sin \varphi + d_R \cos \varphi) - U \frac{2\mu_A}{\rho^2} (c_A \sin \varphi + d_A \cos \varphi). \quad [4.5]$$

A moving meniscus between two parallel plates may be described by the coordinates r and φ (figure 4.2). In this case the wedge angle φ varies along the meniscus. Following

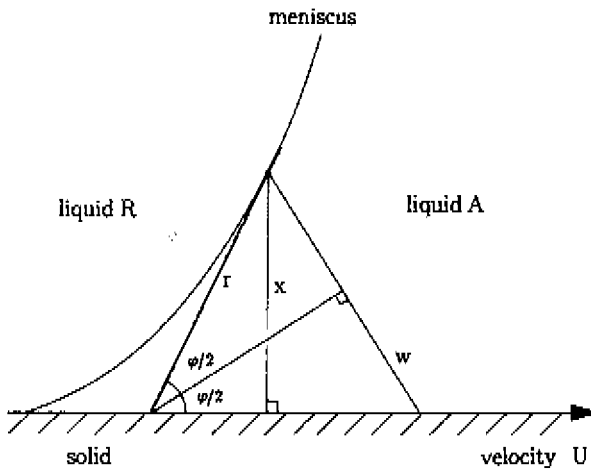


Fig 4.2 Definition of the variables describing a liquid-liquid meniscus.

the approach developed in chapter 2 & 3, the local pressure difference gradient $\partial(p_R - p_A)/\partial s$ (where s denotes arc length along the meniscus) will nevertheless be approximated by that at the interface between two plane wedges having the local inclination φ :

$$\frac{\partial(p_R - p_A)}{\partial s} = U \frac{2\mu_R}{r^2} (c_R \sin \varphi + d_R \cos \varphi) - U \frac{2\mu_A}{r^2} (c_A \sin \varphi + d_A \cos \varphi). \quad [4.6]$$

Denoting the distance from the wall by x , [4.6] may be rewritten as

$$\frac{\partial(p_R - p_A)}{\partial x} = U \frac{2 \sin \varphi}{x^2} (\mu_R c_R \sin \varphi + \mu_R d_R \cos \varphi - \mu_A c_A \sin \varphi - \mu_A d_A \cos \varphi). \quad [4.7]$$

The pressure difference $p_R - p_A$ is balanced by the interfacial tension σ according to Laplace's law:

$$p_R - p_A = \frac{\sigma}{R} = \sigma \frac{d\varphi}{ds} = \sigma \sin \varphi \frac{d\varphi}{dx}, \quad [4.8]$$

where R is the radius of curvature of the meniscus (reckoned positive if the centre of curvature lies on the side of liquid R). The derivative of [4.8] substituted in [4.7] now yields

$$\frac{d}{dx} (\sigma \sin \varphi \frac{d\varphi}{dx}) = U \frac{2 \sin \varphi}{x^2} \varphi \left[\mu_R c_R \sin \varphi + \mu_R d_R \cos \varphi - \mu_A c_A \sin \varphi - \mu_A d_A \cos \varphi \right]. \quad [4.9]$$

Written in term of the capillary number, $Ca (= \mu_A U / \sigma)$ and the viscosity ratio μ_R / μ_A , [4.9] becomes

$$\frac{d}{dx} (\sin \varphi \frac{d\varphi}{dx}) = \frac{2 \sin \varphi}{x^2} \varphi Ca \left[\frac{\mu_R}{\mu_A} c_R \sin \varphi + \frac{\mu_R}{\mu_A} d_R \cos \varphi - c_A \sin \varphi - d_A \cos \varphi \right]. \quad [4.10]$$

Equation [4.10] is the required differential equation describing the shape of the meniscus. Notice that the "constants" c_R, \dots, d_A depend on φ . The equation should constitute a good approximation provided φ varies "slowly", where slowly means something like:

$$\frac{d\varphi/\varphi}{ds/w} \ll 1 \quad [4.11]$$

(w : the local wedge width — figure 4.2).

Axisymmetric geometry

In the manner described in chapter 2, [4.10] can be modified to take account of the

second radius of curvature present in the axis-symmetric (capillary-tube) case, yielding

$$\frac{d}{dx} \left(\sin \varphi \frac{d\varphi}{dx} + \frac{\cos \varphi}{a-x} \right) = \quad [4.12]$$

$$\frac{2 \sin \varphi}{x^2} \text{Ca} \left[\frac{\mu_R}{\mu_A} c_R \sin \varphi + \frac{\mu_R}{\mu_A} d_R \cos \varphi - c_A \sin \varphi - d_A \cos \varphi \right],$$

where a denotes the tube radius.

Condition at the solid boundary

The meniscus equations [4.10] & [4.12] apply sufficiently far from the wall where the fluids behave "classically", being described by the continuum equations together with a constant interfacial tension. Close to the wall (minimally at a distance of the order of molecular dimensions) the continuum approximation inevitably breaks down due to the molecular character of the liquids. As in chapter 2 and 3, this will be modelled in the simplest possible manner, namely that the classical description applies up to a distance λ from the wall, of the order of a molecular dimension, at which point the final (true) value of the contact angle, φ_0 , is attained. Note that the stress singularity otherwise encountered at $x = 0$ does not now arise.

4.3 Solutions of the governing equation

In chapter 2 and 3 only a small difference was found between the shapes of moving menisci in parallel plate and capillary-tube geometry, both in the advancing as in the receding case. Consequently only the shape of a moving meniscus in a capillary will be examined in detail here. The analysis is however readily modified to the corresponding parallel-plate cases.

The meniscus equation [4.12] is solved as indicated in chapter 2, making use of a logarithmic scale of distance

$$\xi = \ln(x/\lambda), \quad [4.13]$$

by numerically integrating from the centre axis ξ_c to the distance λ from the wall ($\xi=0$) using a second-order finite-difference scheme. The subscript c will be used to identify a property on the axis of symmetry and the subscript 0 a property at $\xi=0$. The integration procedure requires the values of φ_c and η_c where

$$\eta = \frac{d\varphi}{d\xi}. \quad [4.14]$$

Symmetry requires that φ_c be 90° .

The apparent or "dynamic" contact angle in the advancing fluid, φ_d , is taken as the angle which a circular meniscus, having the same apex height h as the actual meniscus, would make with the wall (figure 4.3):

$$\varphi_d = \cos^{-1} \left[\frac{2ha}{a^2+h^2} \right]. \quad [4.15]$$

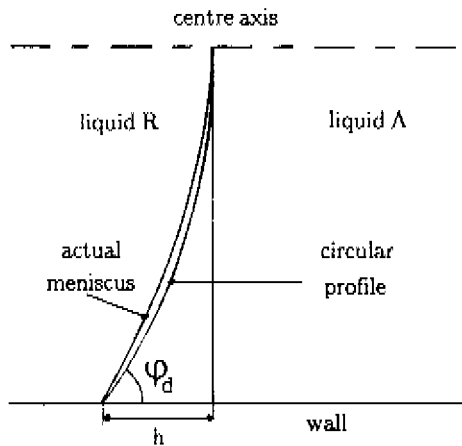


Fig 4.3 Definition of the dynamic contact angle, φ_d .

In figure 4.4 the true advancing contact angle (φ_0), obtained from the solution of [4.12], is presented as a function of η_c ($\mu_R/\mu_A = 10^{-1}$, $Ca = 5 \cdot 10^{-2}$ and $\xi_c = 15^1$). It is

¹The order of magnitude corresponding to tubes of order 1 mm, assuming λ to be of the order of 1 nm.

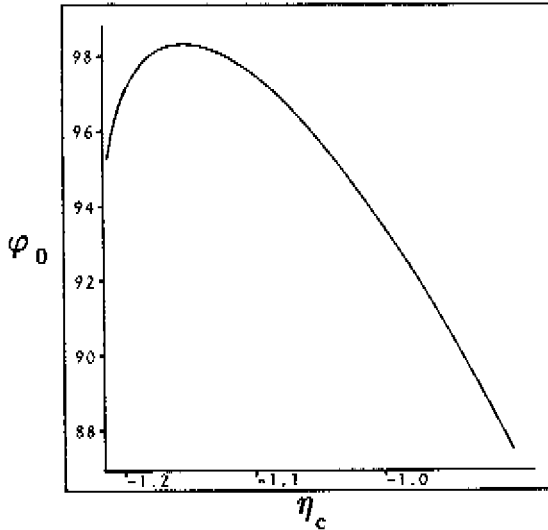


Fig 4.4 Variation of the true contact angle, φ_0 , with the curvature at the axis, η_c ($\mu_R/\mu_A = 10^{-1}$, $Ca = 5 \cdot 10^{-2}$, and $\xi_c = 15$).

observed that φ_0 exhibits a maximum ($\varphi_{0,\max}$). Evidently for $\varphi_0 > \varphi_{0,\max}$ no solution to the meniscus equation [4.12] exists while for $\varphi_0 < \varphi_{0,\max}$ there are two solutions. As in the receding case for the solutions having $d\varphi_0/d\eta_c > 0$ it was found that $d\eta_c/d(Ca) > 0$ (for constant φ_0 , ξ_c and μ_R/μ_A) and consequently that $d\varphi_0/d(Ca) < 0$, which is contrary to experimental findings. The solutions for which $d\varphi_0/d\eta_c > 0$ will therefore be ignored. These solutions are presumably unstable and consequently not encountered in reality.

Another way of looking at this question is to note that for $\varphi_0 = \varphi_{0,\max}$ the capillary number has a critical value ($Ca = Ca_{crit}$) above which no solution to the meniscus equation [4.12] exists.

In figure 4.5 the predicted relation between the critical capillary number and the true contact angle is presented for different values of μ_R/μ_A ($\xi_c = 15$). If the receding phase becomes more viscous the critical capillary number becomes smaller. For a purely

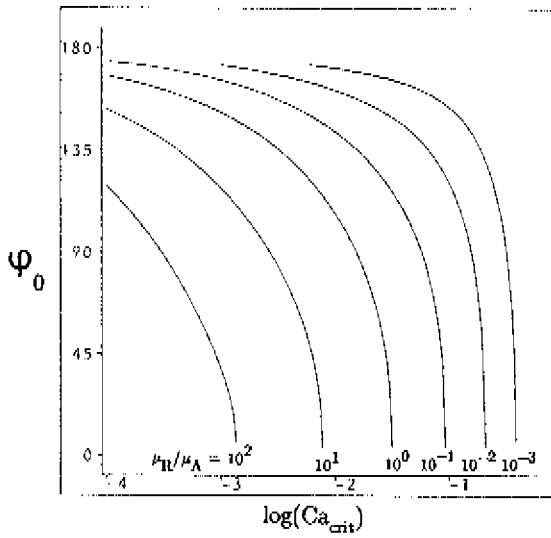


Fig 4.5 The dependence of the critical capillary number on the true contact angle, ϕ_0 , for various viscosity ratios ($\xi_c = 15$).

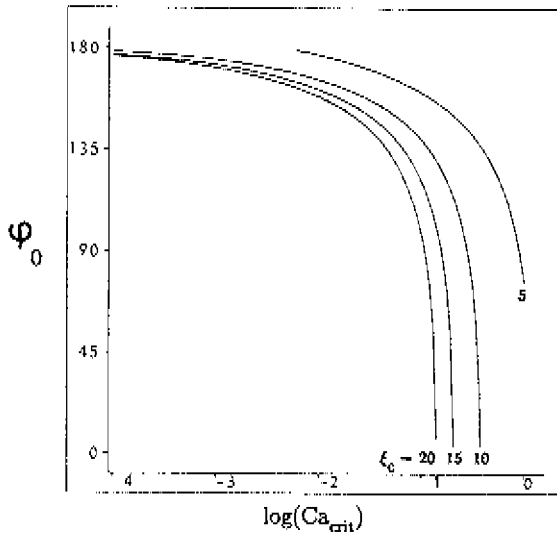


Fig 4.6 The dependence of the critical capillary number on the true contact angle, ϕ_0 , for various system scales ($\mu_R/\mu_A = 10^{-2}$).

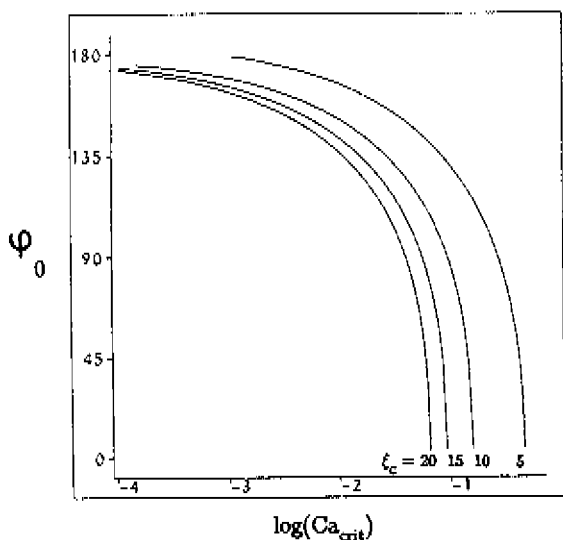


Fig 4.7 The dependence of the critical capillary number on the true contact angle, ϕ_0 , for various system scales ($\mu_R/\mu_A = 10^{-1}$).

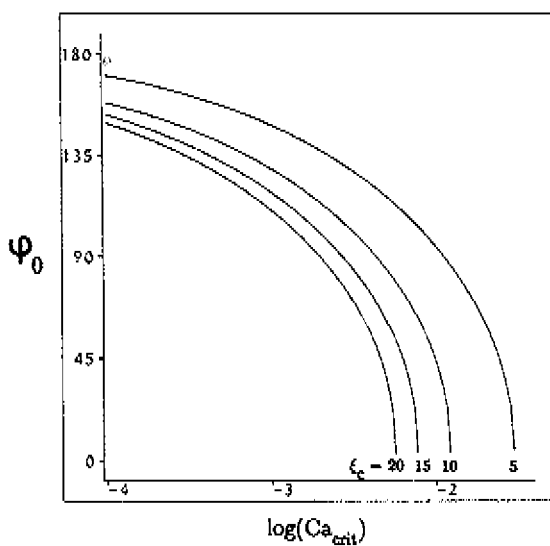


Fig 4.8 The dependence of the critical capillary number on the true contact angle, ϕ_0 , for various system scales ($\mu_R/\mu_A = 10$).

advancing case ($\mu_R/\mu_A = 0$) a solution of the meniscus equation exists for all capillary numbers and all values of the true contact angle. The viscosity of the receding liquid thus limits the range of the possible capillary numbers for which a stable meniscus exists. The ξ_c -dependence of the critical capillary number is presented in figures 4.6, 4.7 and 4.8 for the cases, $\mu_R/\mu_A = 10^{-2}$, $\mu_R/\mu_A = 10^{-1}$ and $\mu_R/\mu_A = 10$ with $\xi_c = 5, 10, 15$ and 20.

4.4 The transition to purely advancing or receding behaviour

Although a "purely" advancing/receding situation, corresponding to zero viscosity of the receding/advancing phase is formally unattainable a close approximation may be expected for sufficiently small/large values of the viscosity ratio μ_R/μ_A . To examine the transition to purely advancing behaviour, the predicted dynamic contact angle is presented in figure 4.9 as a function of the capillary number the viscosity ratios $\mu_R/\mu_A = 10^{-1}, 10^{-2}, 10^{-3}$ and 0 ($\varphi_0 = 45^\circ, \xi_c = 15$). It is seen that while the effect of a receding viscosity $\mu_R = 10^{-1}\mu_A$ may not be neglected, if $\mu_R = 10^{-2}\mu_A$ the moving contact line can be modelled as an advancing contact line except for the higher capillary numbers. For $\mu_R \leq 10^{-3}\mu_A$ the dynamic contact angle behaves as an advancing contact angle.

The transition to purely receding behaviour is examined in figure 4.10, as a function of the receding capillary number ($U < 0$ and consequently $Ca < 0$) for the viscosity ratios $\mu_A/\mu_R = 10^{-1}, 10^{-2}, 10^{-3}$ and 0 ($\varphi_0 = 135^\circ, \xi_c = 15$). While the effect of the advancing viscosity $\mu_A = 10^{-1}\mu_R$ may not be neglected, deviations from purely receding behaviour are again small for $\mu_A = 10^{-2}\mu_R$ and negligible for $\mu_A \leq 10^{-3}\mu_R$.

4.5 Comparison with numerical solutions

The shape of a moving meniscus between two equally viscous liquids ($\mu_A/\mu_R = 1$) in a capillary has been computed for a number of cases by Tilton (1988) using a

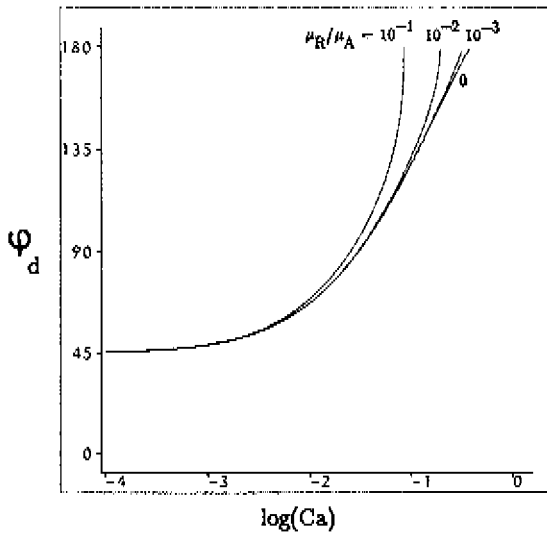


Fig 4.9 The dependence of the dynamic advancing contact angle on the viscosity of the receding fluid ($\xi_c = 15$, $\varphi_0 = 45^\circ$).

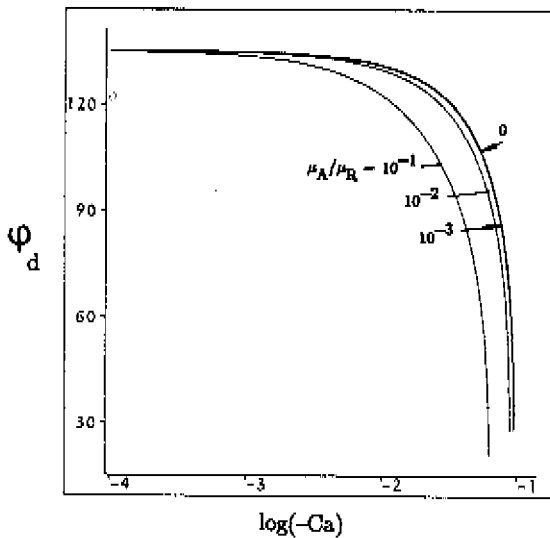


Fig 4.10 The dependence of the dynamic receding contact angle on the viscosity of the advancing fluid ($\xi_c = 15$, $\varphi_0 = 135^\circ$). The line for $\mu_A/\mu_R = 10^{-3}$ almost coincides with the line for $\mu_A/\mu_R = 0$.

finite-element method. In figure 4.11 the largest-Ca cases treated by Tilton (crosses), for various true contact angles, are compared with the results obtained by integration of [4.12] from the tube axis to the wall (continuous lines)² (ξ_c was chosen as 15). The value of η_c has been chosen to optimize the agreement with the results obtained by Tilton.

As noted earlier, Tilton avoided the singularity at the contact line by introducing slip close to the contact line while in this study the singularity was avoided by invoking the breakdown of the continuum description. Close to the wall this difference in boundary condition may therefore result in a poor agreement between Tilton's results and the results obtained here.

In figure 4.11 it is observed that the agreement between the results obtained by Tilton and the solutions of meniscus equation [4.12] is excellent. This comparison however is not a critical test because there are only minor deviations from the spherical to be observed. Where these deviations occur, solutions of meniscus equation [4.12] are nevertheless in good agreement with Tilton's results. At the wall a small discrepancy is seen, which probably is the result of the different boundary conditions at the wall. For smaller capillary numbers the agreement may be expected to be better.

The Ca-dependence of the shape of a moving meniscus between two equally viscous liquids in a capillary has also been investigated by Zhou & Sheng (1990) using a finite-difference method. They too avoided the singularity at the contact line by using a slip model. Their values of $-h/a$ as a function of Ca are compared in figure 4.12 with the predictions of the model ($\mu_A/\mu_R = 1$). It is clear that the model can predict the macroscopic meniscus shape, except possibly for very large Ca.

A comparison with experimental results, as carried out in the next section, may be more revealing and may provide insight into the nature of the boundary condition to be used at the wall.

²Following Tilton, the shape of the moving meniscus is presented here as $1-x/a$ versus $(h-h_{\text{wall}})/a$.

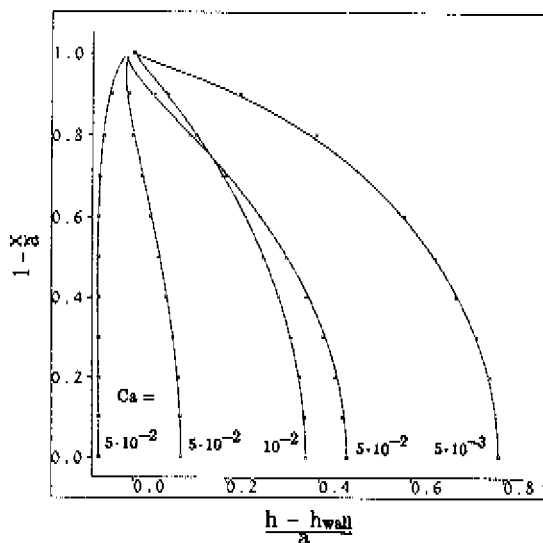


Fig 4.11 Comparison of the solution of the meniscus equation [4.12] (continuous lines) with the results obtained by Tilton (crosses) for the highest capillary numbers investigated and for various true contact angles.

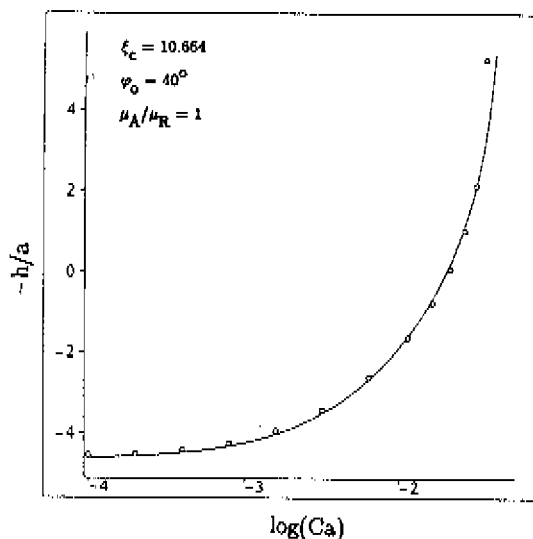


Fig 4.12 Comparison of the results of Zhou & Sheng (squares) with the predictions of the present model (continuous lines, $\xi_c = 10.664$, $\varphi_0 = 40^\circ$, $\mu_A/\mu_R = 1$) giving the Ca -dependence of h/a (the meniscus height).

4.6 Comparison with experimental results

In figure 4.13 measurements performed by Fermigier & Jenffer (1988) of the dynamic contact angle of glycerol displacing a viscous silicon oil ($\mu_R/\mu_A = 9 \cdot 10^{-1}$) and of silicon oil displacing air ($\mu_R/\mu_A = 3.6 \cdot 10^{-6}$) in a capillary are compared with the predictions of the model presented here, based on the supposition that the true contact angle, φ_0 , is constant and equals the static contact angle. λ was taken to be 10^{-9} m. The model exhibits agreement with these experimental results. In figure 4.14 further measurements of the dynamic contact angle of glycerol displacing low and moderate-viscosity silicon oils ($\mu_R/\mu_A = 7.6 \cdot 10^{-3}$ and $\mu_R/\mu_A = 10^{-1}$) are compared with the model ($\varphi_0 = \varphi_s$, $\lambda = 10^{-9}$ m and 10^{-10} m). While agreement between experiment and model could be improved by choosing a much smaller value of λ the only physically realistic possibility is that in the cases in figure 4.14 the true angle at the wall depends significantly on the contact line speed, as was also concluded by Zhou & Sheng (1990). A line speed dependence of the true contact angle has also been suggested by Hoffman (1983). The true contact angle required to obtain agreement between model and experiments, taking $\lambda = 10^{-9}$ m, is shown in figure 4.15. A very similar conclusion also shown in the figure was reached by Zhou & Sheng. As might be anticipated, the implied true contact angle exhibits a strong dependence on the line speed. The mechanism of such line-speed dependence is however unknown and no explanation can at present be advanced for the fact that in the cases depicted in figure 4.13, such dependence is not in evidence.

4.7 Conclusion & discussion

The approach developed earlier to resolve the hydrodynamic problem associated with liquid-gas contact lines is extended here to the liquid-liquid case. Since liquid-liquid contact lines always involve one receding liquid, they share the feature of receding

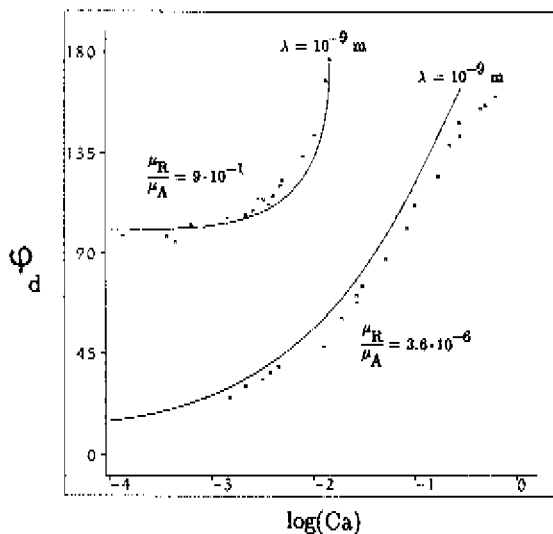


Fig 4.13 Capillary number dependence of the dynamic contact angle as measured by Fermigier & Jenffer (crosses) and as predicted by the meniscus equation [4.12] (continuous lines). Static contact angle = 100° and 12° .

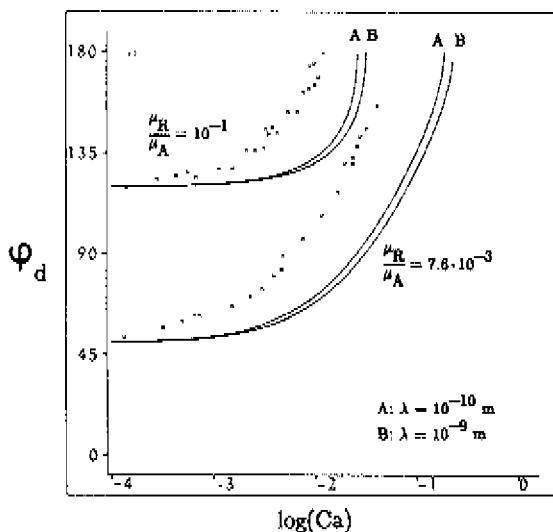


Fig 4.14 Capillary number dependence of the dynamic contact angle as measured by Fermigier & Jenffer (crosses) and as predicted by the meniscus equation [4.12] (continuous lines). Static contact angle = 120° and 50° .

liquid-gas contact lines that beyond a critical capillary number no stationary solution exists.

The agreement of the model with the computations of Zhou & Sheng is excellent and suggests that the models' representation of the hydrodynamics is good. Another test is formed by the experimental results of Fermigier & Jenffer. The good agreement obtained in some but not all cases if it is assumed that $\varphi_0 = \varphi_B$ confirms this impression but suggests that some other factor sometimes enters into the wall boundary conditions. While this additional factor may be a line-speed dependence of the true contact angle, there are other possibilities, such as effects surface inhomogeneities or of trace surfactants.

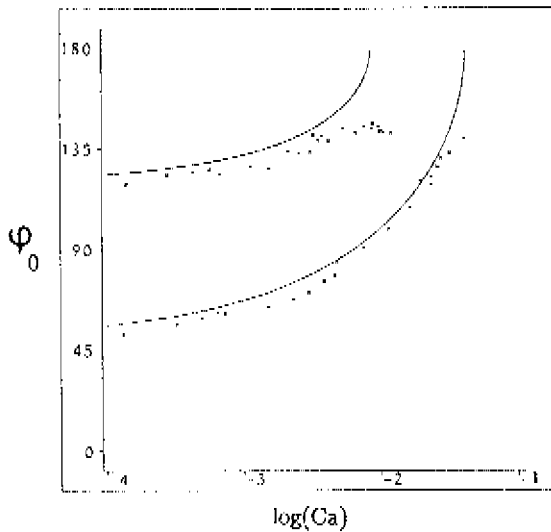


Fig 4.15

Variation of the true contact angle, φ_0 , with Ca required to obtain agreement between computations and experiments: crosses the present model ($\lambda = 10^{-9}$ m), continuous lines computations of Zhou & Sheng.

CHAPTER 5 – *Experimental determination of advancing and receding dynamic contact angles in a capillary tube*

5.1 Introduction

With the exception of the observations of Hansen & Toong (1971), the shape of a moving meniscus inside a capillary tube has been reported to be spherical, for instance by Rose & Heins (1962) or more recently by Hoffman (1975) in the case of an advancing meniscus (liquid displacing a gas) and by Fermigier & Jenffer (1988) in the liquid–liquid case. The velocity dependent dynamic contact angle, φ_d , between the meniscus and the wall then determines the meniscus shape.

The preceding chapters suggest that very close to the wall a significant deviation from the spherical *must* occur as a result of viscous stresses and that this deviation is at least in part responsible for the observed dependence of the dynamic contact angle on the line speed [see for example also Dussen V. (1979) and de Gennes (1985) for relatively recent reviews]. Direct verification of this prediction is not yet available, however, the predicted thickness of the wall region being in general too small to permit visual observation.

As a prelude to the development and application of a technique for determining the meniscus shape close to the wall in the advancing case – reported in chapter 6 – a number of observations of the dynamic contact angle were carried out in both the advancing and receding cases. To arrive at fluids exhibiting non–zero static contact angle (φ_s) on glass capillary tubes, liquid–liquid rather than liquid–gas systems were chosen, using a large viscosity ratio to minimize the role of viscous forces in the less viscous phase. The results of this exercise –reported below – proved of interest in their own right, confirming earlier indications that a significant line–speed dependence of the true contact angle, φ_0 , occurs in

certain cases.

5.2 Experiments

In order to measure dynamic contact angles of a meniscus formed by two liquids in a capillary, a device has been constructed as shown in figure 5.1. With the help of a servo

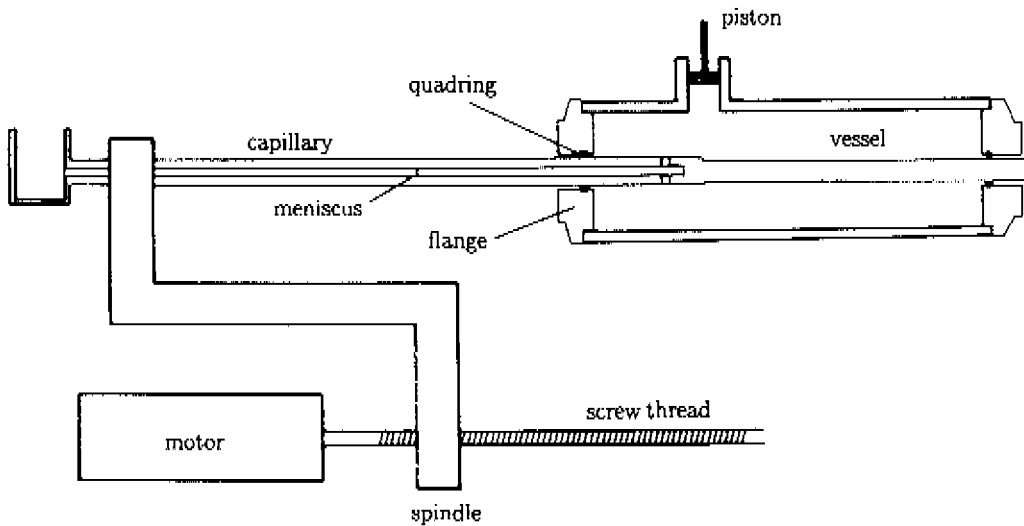


Fig. 5.1 Experimental set-up.

motor a glass capillary and rod combination can be made to move through a vessel filled with liquid. The liquid in the vessel has access to the capillary via two holes in its wall. The dimensions of the capillary and the rod are chosen such as to produce a moving meniscus which moves with respect to the capillary but not with respect to the laboratory frame. The dynamic contact angles were determined by taking photographs and measuring the apex height of the meniscus (equation [4.15]). A microscope slide mounted against the capillary with decalin (having the same index of refraction as glass) in between prevented light refraction from the outer tube wall.

5.3 Results

The first liquid combination used was glycerine ($\mu = 1.47 \text{ kg m}^{-1} \text{ s}^{-1}$) displacing hexane ($\mu = 3.68 \cdot 10^{-4} \text{ kg m}^{-1} \text{ s}^{-1}$, $\mu_R/\mu_A = 2.5 \cdot 10^{-4}$) with interfacial tension $2.52 \cdot 10^{-2} \text{ N m}^{-1}$ (measured by the Wilhelmy plate method). In figure 5.2 the results are

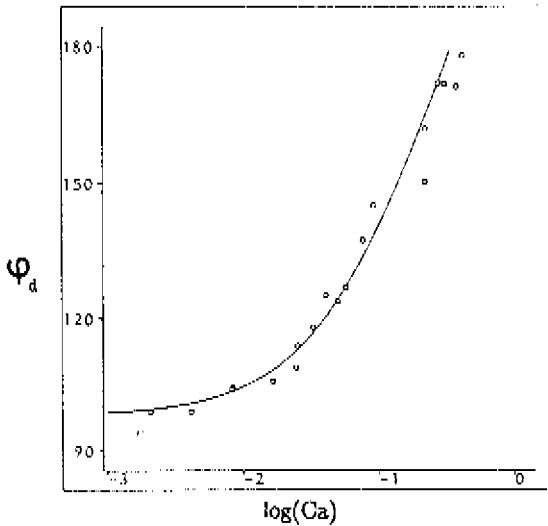


Fig. 5.2 The Ca -dependence of φ_d for glycerine displacing hexane ($a = 8.61 \cdot 10^{-4} \text{ m}$).

compared with the model outlined in chapter 4 taking $\lambda = 10^{-9} \text{ m}$ and $\varphi_0 = 98^\circ$. The agreement is good, implying that in this case the approximation of constant φ_0 is acceptable.

The second liquid combination used was glycerine ($\mu = 0.995 \text{ kg m}^{-1} \text{ s}^{-1}$) displacing a low viscous silicon oil ($\mu = 4.79 \cdot 10^{-3} \text{ kg m}^{-1} \text{ s}^{-1}$, $\mu_R/\mu_A = 4.81 \cdot 10^{-3}$) with interfacial tension $1.99 \cdot 10^{-2} \text{ N m}^{-1}$ (measured by the pendent drop method). In figure 5.3 the results are compared with the model taking $\varphi_0 = 66^\circ$ and $\lambda = 10^{-9} \text{ m}$ or 10^{-10} m .

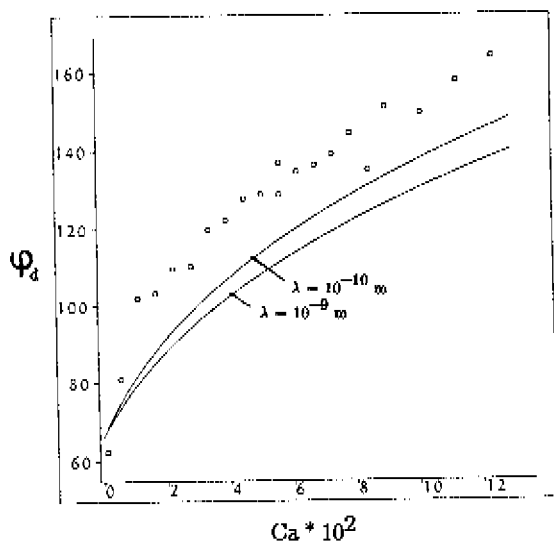


Fig. 5.3 The Ca -dependence of ϕ_d for glycerine displacing a low viscous silicon oil ($a = 8.28 \cdot 10^{-4} \text{ m}$).

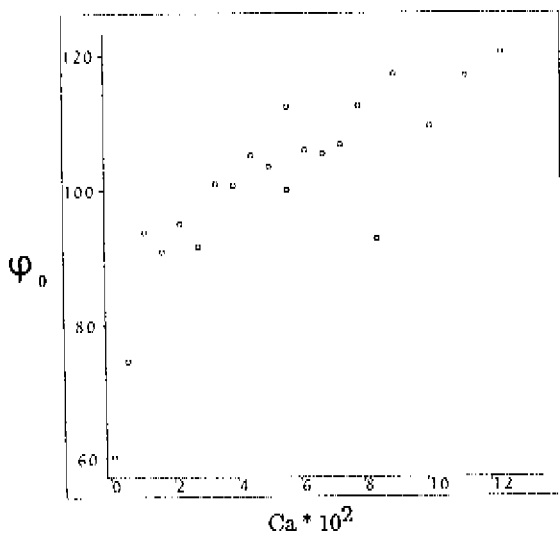


Fig. 5.4 Variation of ϕ_0 with Ca required to obtain agreement between computations and experiments in the case studied in figure 5.3.

The measurements deviate significantly from the predictions of the model. The agreement could be improved by choosing a smaller λ -value. However, in view of the size of the molecules this would be physically unacceptable. A more obvious choice which leads to better agreement is to abandon the assumption that the true contact angle remains equal to the static value. In figure 5.4 the true contact angle at the wall needed to obtain agreement between model ($\lambda = 10^{-9}$ m) and experiments is presented as a function of the capillary number.

Finally the same liquid combination was used with the silicon oil as the advancing liquid and the glycerine as the receding. In figure 5.5 the measurements are shown to agree with the predictions of the model, taking $\varphi_0 = 38^\circ$ and λ around $6 \cdot 10^{-9}$ m.

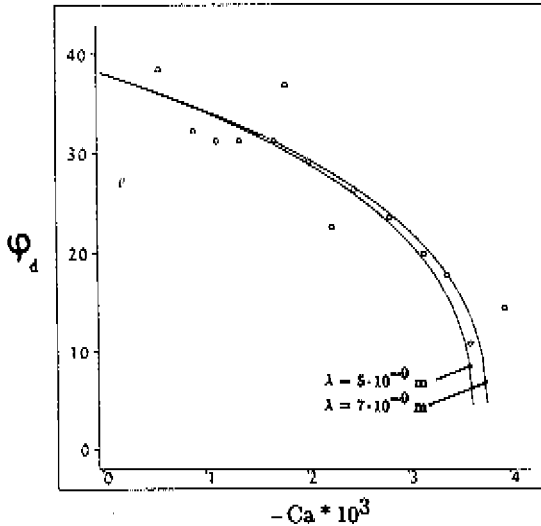


Fig. 5.5 The Ca -dependence of φ_d (here measured in the receding phase) in the same case as studied in figure 5.3 except a reversal of the line speed. (Here $Ca = \mu_R U / \sigma$.)

5.4 Discussion

The present measurements on liquid–liquid systems extend those of Fermigier & Jenffer (1988), discussed in chapter 4, in which the largest value of μ_R/μ_A was 0.9 (as compared with around 200 in the present study) and the smallest $7.6 \cdot 10^{-3}$ (as compared with $2.5 \cdot 10^{-4}$ here). The comparison of the new data with predictions of the model provides the same picture, however: in some cases the behaviour is adequately predicted taking $\varphi_0 = \varphi_s$, in others a significant increase in φ_0 (measured in the advancing phase) with Ca must be supposed in order to obtain agreement.

The results for the same pair of liquids in both the advancing and the receding modes indicate that considerable hysteresis (28°) exists in the static contact angle. The presence of hysteresis points to non-ideality of the wall (roughness/chemical heterogeneity). Since this feature is not included in the model, it is conceivable that it, rather than a deviation of φ_0 from φ_s , is responsible for the discrepancy between model and measurements.

Finally it should be noted that the fact that the advancing mode of the glycerine–silicon oil system exhibits a deviation of φ_0 from φ_s , while the receding mode does *not* should not be considered significant: the largest Ca–values in the receding case are less than those at which significant deviation is observable in the advancing case.

CHAPTER 6 – *Experimental determination of the meniscus curvature in the vicinity of an advancing liquid–gas contact line*

6.1 Introduction

As discussed briefly in chapter 5, all models of the hydrodynamics of moving fluid–fluid–solid contact lines predict a significant deformation of the meniscus as the line is approached as a result of viscous stresses. Indeed, were the classical approximations of no slip, of an interfacial tension and of the continuum description to apply at all distances from the line, this deformation would be indefinitely large at all non–zero line speeds.

In reality, at least the continuum approximation must lose its validity at distances from the solid of the order of a molecular dimension, thereby removing the singularity and limiting the extent of the deformation. In addition, significant slip may occur, as supposed by many authors [Dussan V. (1976), Huh & Mason (1977), Cox (1986)] and as suggested by simple molecular–dynamics simulation [Thompson & Robbins (1989)], while the approximation of an interfacial tension, confined to an indefinitely thin layer, must be replaced, close to the line, by a representation of the long–range inter–molecular interactions as volume forces. The latter exercise has recently been carried out for a system exhibiting a small but non–zero contact angle, taking account of van der Waals interactions [de Gennes, Hua & Levinson (1990)]. Like the effects of the discontinuous nature of matter and of slip, this deviation from the classical approximations is predicted to limit the meniscus deformation, becoming the dominant effect for very small static contact angles (see section 6.5). Finally, in addition to the above effects, a deviation of the true contact angle from its static value may occur, associated for example with the adsorption and desorption processes involved in the displacement of the contact line.

From the foregoing it is evident that observations of the meniscus shape close to the contact line in specific cases would be extremely helpful in sorting out the occurrence and relative importance of the various effects. Since, however, the thickness of the region adjoining a moving contact line in which the meniscus is significantly deformed is too small for this deformation to be verified visually this requires special techniques.

Using a microscope, the first part of this wall region was observed by Dussan V., Ramé & Garoff (1991), at a distance of between $3 \cdot 10^{-4}$ and $2 \cdot 10^{-5}$ m from the wall, for an advancing meniscus formed by immersing a glass cylinder in silicone oil.

At molecular distances from the wall the shape of a liquid-gas interface of a spreading drop has been measured via ellipsometry by Heslot, Cazabat & Levinson (1989), Heslot, Fraysse & Cazabat (1989), Heslot, Cazabat & Fraysse (1989) and Heslot, Cazabat, Levinson & Fraysse (1990). These experiments showed clearly a "step-like" shape very close to the contact line which was supposed to be a result of the layering of the molecules.

In this chapter a new technique is described by which the curvature of an advancing meniscus in a capillary tube has been measured down to around 50 nm from the wall: sufficiently close to cover the greater part of the deformed region.

The results described in this chapter are compared with the predictions of the model described in chapter 2, in which the only incorporated deviation from classical behaviour is the breakdown of the continuum approximation, the classical two-phase equations being solved down to a distance, λ , from the solid, at which point the wall is supposed to have been reached and with it the final meniscus inclination, or true contact angle, φ_0 . (The value of λ required to fit data on advancing dynamic contact angles was indeed found to be of the order of a molecular dimension: $\lambda \sim 10^{-9}$ m.)

6.2 Experimental set-up

The measuring technique makes use of a parallel laser beam which uniformly

illuminates a part of the curved interface (see figure 6.1). Neglecting wave effects the

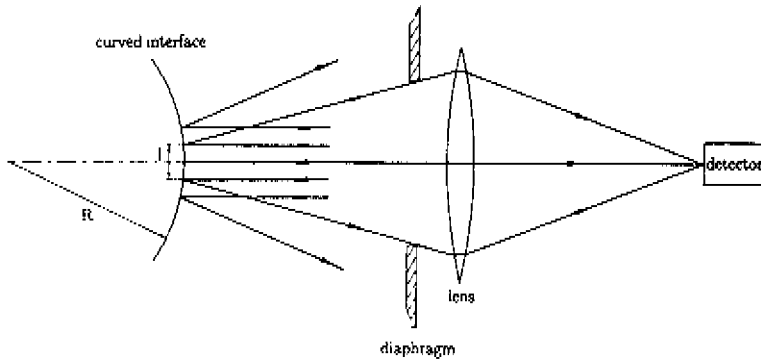


Fig. 6.1 The basis of the measuring technique used for measuring the curvature of a (partially) reflecting curved interface.

reflected light which passes a diaphragm and is focused on a detector originates from a portion of the illuminated interface of length l . Only those rays pass the diaphragm whose inclination to the system axis lies within a certain angle (of the order of a degree). The detected intensity is proportional to l , which in turn is proportional to the radius of curvature, R , of the interface since the distance between the interface and the diaphragm is much larger than R (the light originates from a virtual source close to the interface). Extending this reasoning to include curvature in the perpendicular plane the detected intensity is seen to be proportional to R_1R_2 , where R_1 and R_2 are the relevant radii of curvature of the interface.

The heart of the experimental setup is a glass capillary with external diameter 6.0 mm and internal diameter 1.7 mm which is partially filled with liquid. This capillary can move in and out a vessel which is filled with the same liquid (see figure 6.2). A movement of the capillary into the vessel, imposed by a servo motor, causes the liquid-gas meniscus in the capillary to advance in the opposite direction.

The capillary tube is actuated on a stepper motor (figure 6.3). An almost parallel

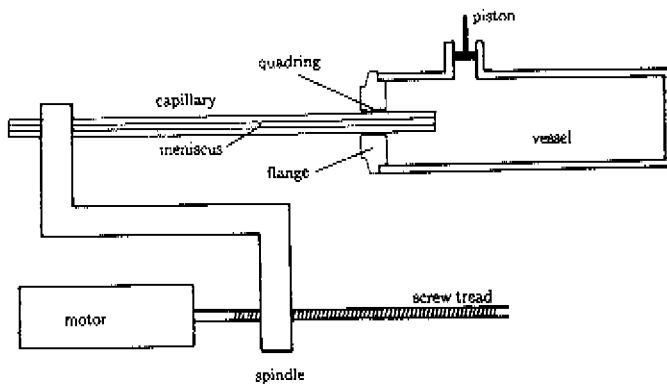


Fig. 6.2 System used to create the advancing meniscus.

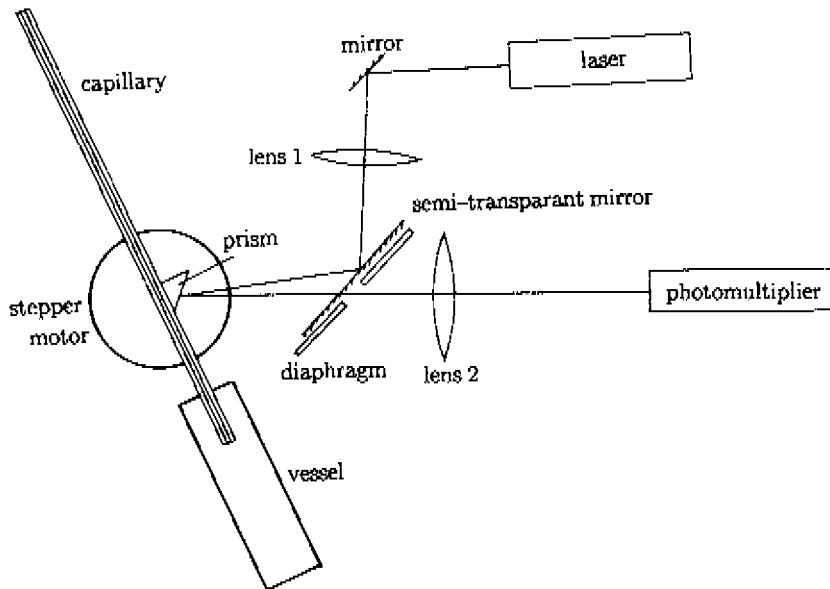


Fig. 6.3 Overall set-up.

laser beam illuminates a small portion of the meniscus, lens 1 determining the size of the illuminated spot. The spot size must not be too small as the measuring technique is based on the assumption that the portion of the meniscus from which the reflected intensity is measured is uniformly illuminated. The prism mounted against the capillary permits the required range of angles of incidence. Between the prism and the capillary a drop of decalin (refractive index equal to that of the glass) prevented refraction on the outer tube wall. The angle between the laser beam impinging on the meniscus and the reflected rays through the diaphragm was not zero but approximately 5° . This was done to avoid scattered light from the laser beam incident on the semi-transparent mirror entering the photomultiplier. A small mirror, instead of the semi-transparent mirror, could also have been used.

6.3 Measuring procedures

To insure cleanliness, the capillary and the inside of the vessel were first washed with chromic acid. Afterwards both were rinsed with distilled water and dried in an oven for about half an hour at around 120° C. The vessel was then filled with silicon oil of moderately high viscosity (dynamic viscosity, μ , = $0.552 \text{ kg m}^{-1} \text{ s}^{-1}$, surface tension, σ , = $2.22 \cdot 10^{-2} \text{ N m}^{-1}$, static contact angle 0°). The use of a much higher viscosity would have required very small velocities for a given capillary number, ($Ca = \mu U / \sigma$, U contact line speed with respect to the solid). Temperature fluctuations of the liquid in the vessel would then superimpose a comparable additional velocity. The use of a much smaller viscosity could have led to inertial effects, which are not included in the theoretical model.

The moving meniscus traverses the laser beam and the intensity of reflected light is measured. The intensity detected by the photomultiplier shows a peak as the meniscus passes the laser beam (figure 6.4). At the moment the maximum intensity, I_{\max} , is registered, the meniscus is in the centre of the laser beam. As was argued before, I_{\max} is

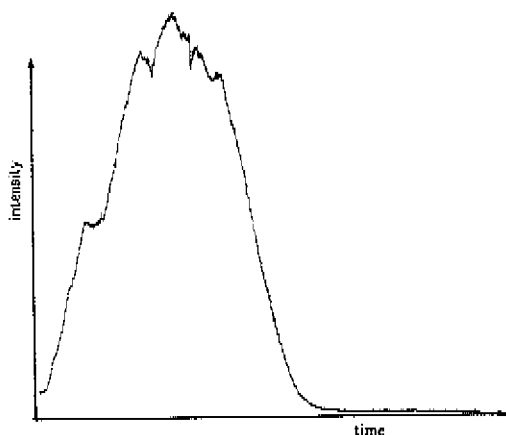


Fig. 6.4 Intensity record of the reflected light during the passage of a meniscus through the laser beam.

proportional to the product of the radii of curvature. To obtain this product, the system was calibrated using known radii of curvature. For this purpose a very slowly receding meniscus was used. Although a thin film is left behind, the (equal) radii of curvature of a slowly receding meniscus are very nearly equal to that of the capillary, a .

A contact line formed by a liquid with zero static contact angle cannot recede. Thus a given region of the capillary can be used only once. To carry out further measurements, the capillary and the vessel in figure 3 can be displaced so that the laser beam shines on a dry part of the capillary. The measurement of the advancing meniscus can then be repeated followed by calibration with the slowly "receding" meniscus. After each measurement of an advancing meniscus follows a measurement of a "receding" meniscus.

The stepper motor in figure 6.3 can rotate the capillary and the vessel so that there can be measured at different angles.

To avoid stick-slip phenomena between the quadrant and the capillary (figure 6.2), the outside of the capillary which moves into the vessel is prewetted with the silicon oil as used for the meniscus. This lubrication makes a smoother motion of the meniscus possible.

Even then, not every record of intensity was as smooth as in figure 6.4. Intensities with a more "ragged" appearance, as depicted in figure 6.5, were also registered.

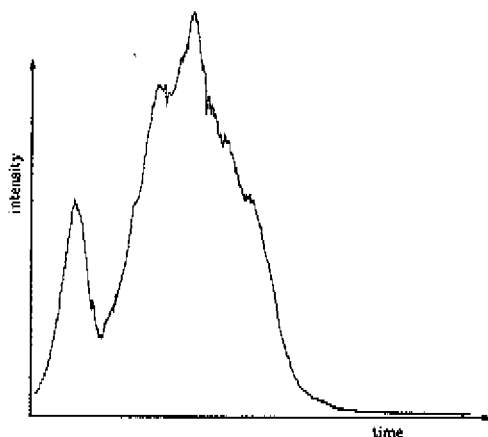


Fig. 6.5 More ragged intensity record of the reflected light during the passage of a meniscus through the laser beam.

When all the dry regions of the capillary had been used it was first rinsed with hexane and then with water, after which the washing procedure with chromic acid and distilled water was repeated. All measurements were performed with the same capillary over a length of approximately 20 cm.

6.4 Results

In figure 6.6 the results of the measurements for $Ca = 6.40 \cdot 10^{-3}$ are presented (the error bars), together with the predictions of the model for various λ -values, taking the true contact angle, φ_0 as constant at 0° . Every bar is the result of at least ten measurements. φ , which is determined by the angle of incidence of the laser beam, denotes the local inclination of the meniscus, varying from 90° at the tube centre to φ_0 at the wall. The term $R_1 R_2 / a^2$, an inverse measure of the meniscus curvature, is constant in the central, spherical

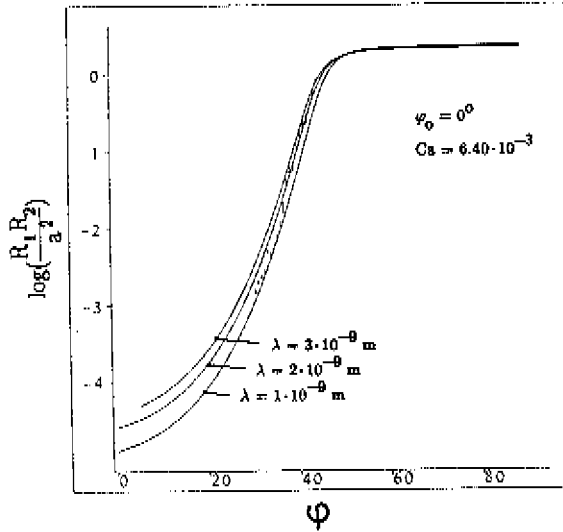


Fig. 6.6 Comparison of the experimental results (error bars) with the prediction of the model for three λ -values (continuous lines), for given Ca and varying ϕ .

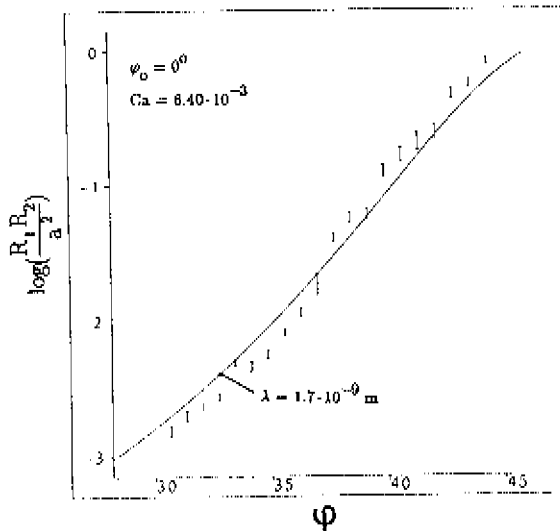


Fig. 6.7 Comparison of the experimental results (error bars) with the best fit of the prediction of the model ($\lambda = 1.7 \cdot 10^{-9}$ m), for given Ca and varying ϕ .

portion of the meniscus and decreases in the wall region. The best fit is obtained for a λ -value of $1.7 \cdot 10^{-9}$ m (figure 6.7). A small systematic deviation remains.

Figure 6.8 presents complimentary measurements at a fixed value of φ for various Ca -values. The corresponding model predictions are once more based on $\lambda = 1.7 \cdot 10^{-9}$ m and $\varphi_0 = 0^0$. A similar deviation is observed, the model overestimating the smaller values of $R_1 R_2$ and underestimating the larger.

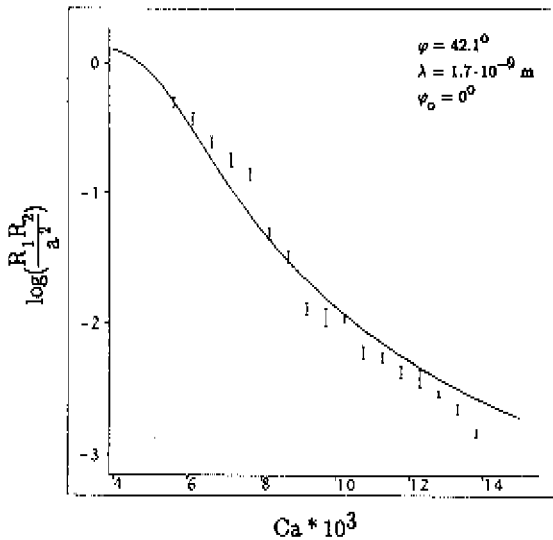


Fig. 6.8 Comparison of the experimental results (error bars) with the prediction of the model ($\lambda = 1.7 \cdot 10^{-9}$ m), for given φ and varying Ca .

The limit of measurable intensity was posed by the background intensity which ultimately becomes comparable with that of the reflection peak, as illustrated in figure 6.9. In the series presented in figure 6.7, the final measurement point corresponds to $x = 4.6 \cdot 10^{-8}$ m and $R_1 = 1.5 \cdot 10^{-6}$ m, where x (distance from the wall) and R_1 have been calculated with the help of the model. For the series in figure 6.8, the corresponding figures are respectively $8.3 \cdot 10^{-8}$ m and $1.7 \cdot 10^{-6}$ m. Since these R_1 -values are only a few times

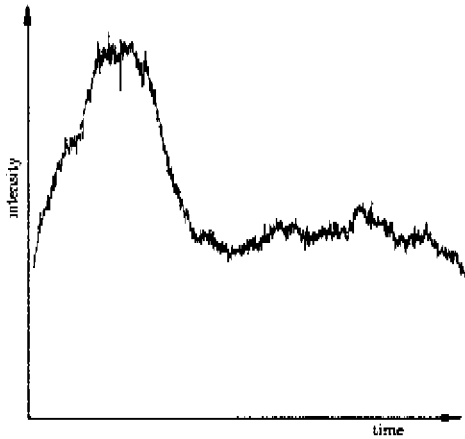


Fig. 6.9 *Intensity of the reflected light during the passage of a meniscus through the laser beam for the smallest measured radius of curvature.*

the wavelength of the laser light, it is likely that wave (i.e. diffraction) effects are becoming significant and the interpretation of the signal then becomes difficult anyway.

6.5 Discussion and conclusions

The results provide direct confirmation of the deformation of an advancing meniscus in the wall region, indicating that at least part of the difference observed between dynamic and static contact angles is indeed apparent rather than real.

Since the measurements do not extend to within molecular distances of the wall it cannot be concluded that the *entire* difference is apparent, as the true contact angle, φ_0 , may not be zero. In the first series of measurements, however (figures 6.6 & 6.7), φ_0 is evidently less than 31° , probably much less in view of the fact that the last measurement point, at $\varphi = 31^\circ$, is around 50 nm from the wall (note that this distance calculated with the help of the model, is independent of the value of φ_0 concerned). If it is supposed that φ_0

is in any case less than 20° then the new best-fit value of λ becomes at most about a factor of 2 larger. This leads to the important conclusion that in the present case the length scale governing the meniscus shape in the wall region is of the order of a nanometer.

At first sight this conclusion would appear to be in conflict with the expectations of de Gennes et al. (1990), who considered the effects of van der Waals forces on the meniscus shape close to the contact line. In the small-Ca limit their equation for the meniscus shape corresponds to [2.46] with approximation [2.30] ($Ca' \approx Ca$) (see appendix E), the role of the length scale λ now being played by the parameter $L/(2\varphi_s^2)$, where L is the lengthscale $\sqrt{A/(6\pi\sigma)}$ (A : the Hamaker constant). Since A is typically of the order of 10^{-20} J, this length scale should be the dominant one for small φ_s -values, becoming greater than 10 nm for φ_s -values less than about 5° . The present case, of *zero* φ_s is, however, excluded by their theory.

Turning now to the difference between the measurements and the model, the first possibility is that this is due to the hydrodynamic approximations of the model. Comparisons of the model with the full numerical solutions of Lowndes (1980), however, indicated that its accuracy is too high for this to be the case (chapter 2).

Another possibility is that the true contact angle increases with the line speed, as suggested by certain measurements on receding contact lines and liquid-liquid systems (chapter 3 & 4). While this might improve the agreement between the measurements and the predictions of figure 6.8, it would not do so for those of figure 6.7.

The final possibility would appear to be some systematic error in the measurement technique, for example due to wave (i.e. diffraction) effects. No attempt has as yet been made either to assess or to correct for such effects.

An attempt was also made to apply the technique to a receding liquid-gas contact line. It did not, however, prove possible to obtain any information on the meniscus shape in the wall region: a receding meniscus with a static contact angle below 90° can have two points on the meniscus on which the laser light impinges perpendicularly: one in the outer

region of the meniscus and one in the wall region. The light reflected on to the photomultiplier from the point in the wall region is drowned by that from the point in the outer region.

CHAPTER 7 – *Conclusion & final remarks*

An approach has been developed to study the hydrodynamics associated with moving fluid–liquid contact lines. The hydrodynamic problem is simplified by applying a local–wedge approximation and the result is a second–order ordinary differential equation for the shape of the meniscus which is readily integrated numerically. Comparisons with available full numerical solutions, as found in the literature, confirm the validity of the meniscus equation up to values of the capillary number of order 10^{-1} .

In the model two phenomenological parameters are used. The first parameter, λ , denotes the smallest distance from the wall where the model is still valid. Closer to the wall at least one of the assumptions on which the model is based must break down in order to avoid a singularity at the contact line. In contrast with many authors who proposed the relaxation of the no–slip condition, the present model abandons the continuum approximation, the final meniscus inclination, φ_0 , being supposed to be reached at the distance λ from the wall. Up to now the values of λ and φ_0 can at best be established by optimizing the agreement between the theoretical predicted meniscus shape and the experimental observed.

Comparison of the dynamic contact angle in the purely advancing case (when a gas is the receding phase) as predicted by the model and as reported in the literature suggests that λ and φ_0 are sufficiently approximated by respectively 10^{-9} m (the order of a molecular dimension) and the static contact angle, φ_s . A sensitivity analysis, however, has shown that the dynamic contact angle is rather insensitive to the precise values of these parameters.

In contrast, the dynamic contact angle in the purely receding case (when a gas is the advancing phase) is predicted to be sensitive to the values of λ and φ_0 . Comparison of the

prediction of the critical capillary numbers with the measurements of Quéré suggests that λ is again of the order of a molecular dimension but that φ_0 deviates from φ_E . It is not, however, clear how much weight should be placed on this conclusion as the model is based on an ideal situation of a smooth, homogeneous surface which, according to the observed contact angle hysteresis, is absent in the experiments of Quéré.

Comparison of dynamic contact angles in the liquid-liquid case as predicted by the model and as measured in experiments reported in the literature and reported in chapter 5 show the strange feature that φ_0 seems to deviate from φ_E in one case while in another case it does not. On this issue more research needs to be done. For instance, could the apparent change in φ_0 be caused by the presence of trace quantities of surfactants, which are known to readily affect many interfacial phenomena (bubble rise velocity, bubble-drop coalescence processes...).

The difference between the dynamic contact angle and the true contact angle is the result of the total deformation in the wall region. It has been shown in chapter 6 that with the light reflection technique it is possible to measure the meniscus shape in the wall region. These measurements once again confirm that λ is of a molecular dimension. In order to extend the reliability of these measurements it would be desirable to be able to take into account the effects of the wave character of the light. This technique could also be used on a receding meniscus if the static contact angle were larger than 90° .

In summary, to arrive at a proper description of the hydrodynamics associated with moving contact lines in most practical situations, more research needs to be done. The most important issues that need attention are the influence of surface roughness/heterogeneity and the presence of surfactants. Another point that has to be considered is the influence of the wave character of the light as used in chapter 6. The methods established here of the local-wedge approximation and the light reflection technique can be regarded as two convenient tools in this further research.

APPENDIX A – Normal stress at the free surface of a creeping flow in a plane wedge

The stream function Ψ of a creeping liquid flow in a plane wedge as used in this thesis is written in polar coordinates ρ and θ as

$$\Psi = \rho F(\theta), \quad [\text{A.1}]$$

where $F(\theta)$ is a function of θ .

The stress tensor, σ_{ij} , for an incompressible liquid can be written according to Batchelor (1967) with the Kronecker delta tensor, δ_{ij} , and the rate-of-strain tensor, e_{ij} , as

$$\sigma_{ij} = -p \delta_{ij} + 2 \mu e_{ij}, \quad [\text{A.2}]$$

where p is the pressure and μ the dynamic viscosity of the liquid. From this follows the normal stress at the free surface of a plane wedge:

$$\sigma_{\theta\theta} = -p + 2 \mu \left(\frac{1}{\rho} \frac{\partial v_\theta}{\partial \theta} + \frac{v_\rho}{\rho} \right), \quad [\text{A.3}]$$

where v_θ and v_ρ are the components of the velocity. Equation [A.3] can be written with the stream function as

$$\sigma_{\theta\theta} = -p + 2 \mu \left[\frac{1}{\rho} \frac{\partial}{\partial \theta} \left(\frac{-\partial \Psi}{\partial \rho} \right) + \frac{1}{\rho^2} \frac{\partial \Psi}{\partial \theta} \right]. \quad [\text{A.4}]$$

From [A.1] and [A.4] follows that the second term on the right hand side of [A.4], the deviatoric component, equals zero and that

$$\sigma_{\theta\theta} = -p. \quad [\text{A.5}]$$

APPENDIX B – *Pressure gradient along the free surface of a creeping flow in a plane wedge*

The ρ component of the Navier–Stokes equation in polar coordinates ρ and θ for a viscous flow is (written with the velocity components v_ρ and v_θ)

$$\frac{\partial p}{\partial \rho} = \mu \left[\frac{1}{\rho} \frac{\partial}{\partial \rho} \left(\rho \frac{\partial v_\rho}{\partial \rho} \right) + \frac{1}{\rho^2} \frac{\partial^2 v_\rho}{\partial \theta^2} - \frac{2}{\rho^2} \frac{\partial v_\rho}{\partial \theta} - \frac{v_\rho}{\rho^2} \right], \quad [\text{B.1}]$$

or written with the stream function Ψ

$$\frac{\partial p}{\partial \rho} = \mu \left[\frac{1}{\rho} \frac{\partial}{\partial \rho} \left(\rho \frac{\partial \left(\frac{1}{\rho} \frac{\partial \Psi}{\partial \theta} \right)}{\partial \rho} \right) + \frac{1}{\rho^2} \frac{\partial^2 \left(\frac{1}{\rho} \frac{\partial \Psi}{\partial \theta} \right)}{\partial \theta^2} + \frac{2}{\rho^2} \frac{\partial \left(\frac{\partial \Psi}{\partial \rho} \right)}{\partial \theta} - \frac{\partial \Psi}{\rho^3} \right], \quad [\text{B.2}]$$

where p is the pressure and μ the dynamic viscosity of the liquid. Equation [B.2] is the tool used in this thesis to calculate $\frac{\partial p}{\partial \rho}$.

APPENDIX C – Numerical solution of a meniscus equation

As an example the procedure of solving equations [2.17] & [2.18] is described. The equations are solved by making steps $\Delta\xi$ and approximating φ and η with second-order accuracy. New values of ξ , φ and η (index n) are calculated from the old values:

$$\xi_n = \xi + \Delta\xi, \quad [C.1]$$

$$\varphi_n = \varphi + \frac{d\varphi}{d\xi} \Delta\xi + \frac{d^2\varphi}{d\xi^2} (\Delta\xi)^2 / 2, \quad [C.2]$$

$$\eta_n = \eta + \frac{d\eta}{d\xi} \Delta\xi + \frac{d^2\eta}{d\xi^2} (\Delta\xi)^2 / 2. \quad [C.3]$$

In [C.2] the required expression for $\frac{d\varphi}{d\xi}$ and $\frac{d^2\varphi}{d\xi^2}$ are [2.17] and [2.18] respectively. In [C.3] $\frac{d^2\eta}{d\xi^2}$ is calculated analytically by differentiating [2.18]. When extended to the liquid-liquid case the expression for $\frac{d\eta}{d\xi}$ is more complex and $\frac{d^2\eta}{d\xi^2}$ is then calculated numerically:

$$\frac{d^2\eta}{d\xi^2} = \left(\frac{d\eta}{d\xi} \Big|_n - \frac{d\eta}{d\xi} \right) / \Delta\xi. \quad [C.4]$$

In calculating the values of φ_n and η_n errors are made by omitting the higher order terms in the Taylor series. These terms are dominated by the third order terms in the series. The change in φ and η is dominated by the first order terms. Thus the relative errors in the change of φ and η can be assessed as respectively

$$\text{Error}(\varphi) = \frac{\frac{d^3\varphi}{d\xi^3} (\Delta\xi)^2}{6 \frac{d\varphi}{d\xi}} \quad [C.5]$$

and

$$\text{Error}(\eta) = \frac{\frac{d^3\eta}{d\xi^3} (\Delta\xi)^2}{6 \frac{d\eta}{d\xi}}, \quad [C.6]$$

from which the step size $\Delta\xi$ is calculated, given a maximal acceptable $\text{Error}(\varphi)$ and $\text{Error}(\eta)$, $\frac{d^3\eta}{d\xi^3}$ being determined numerically.

Appendix D – The values of the coefficients $a_{\mathbf{R}}, \dots, d_{\mathbf{A}}$

The coefficients $a_{\mathbf{R}}, \dots, d_{\mathbf{A}}$ were found by Huh & Scriven (1971) to be:

$$a_{\mathbf{R}} = -1 - \pi c_{\mathbf{R}} - d_{\mathbf{R}}, \quad [\text{D.1}]$$

$$b_{\mathbf{R}} = -\pi d_{\mathbf{R}}, \quad [\text{D.2}]$$

$$c_{\mathbf{R}} = S^2 [S^2 - \delta \varphi + R(\varphi^2 - S^2)]/D, \quad [\text{D.3}]$$

$$d_{\mathbf{R}} = S C [S^2 - \delta \varphi + R(\varphi^2 - S^2) - \pi \tan \varphi]/D, \quad [\text{D.4}]$$

$$a_{\mathbf{A}} = -1 - d_{\mathbf{A}}, \quad [\text{D.5}]$$

$$b_{\mathbf{A}} = 0, \quad [\text{D.6}]$$

$$c_{\mathbf{A}} = S^2 [S^2 - \delta^2 + R(\delta\varphi - S^2)]/D, \quad [\text{D.7}]$$

$$d_{\mathbf{A}} = S C [S^2 - \delta^2 + R(\varphi\delta - S^2) - R \pi \tan \varphi]/D, \quad [\text{D.8}]$$

where $S \equiv \sin \varphi$, $C \equiv \cos \varphi$, $\delta \equiv \varphi - \pi$, $R \equiv \mu_{\mathbf{R}}/\mu_{\mathbf{A}}$ and

$$D \equiv (SC - \varphi)(\delta^2 - S^2) + R(\delta - SC)(\varphi^2 - S^2). \quad [\text{D.9}]$$

It deserves mentioning that Huh & Scriven use the stream function Ψ as in

$$v_{\rho} = -\frac{1}{\rho} \frac{\partial \Psi}{\partial \theta}, \quad v_{\theta} = \frac{\partial \Psi}{\partial \rho},$$

where v_{ρ} and v_{θ} denote the velocities in ρ and θ direction respectively.

Appendix E -- *Comparison of the model of de Gennes with the present model*
(for small Ca)

Taking account of van der Waals forces, de Gennes et al. derived an expression for the meniscus shape in the region where the classical hydrodynamic approximations apply, for the limiting case of small values of the parameters φ_s and $3 Ca/\varphi_s^3$:

$$\varphi = \varphi_s \left[1 + \frac{3Ca}{\varphi_s^3} \ln\left(\frac{x}{\lambda}\right) \right] \quad [E.1]$$

where

$$\lambda = 2 \frac{\sqrt{A}}{\varphi_s^2 \sqrt{(6\pi\sigma)}} \quad [E.2]$$

Making use of the fact that $3 Ca/\varphi_s^3 \ll 1$, this equation can be written

$$\varphi^3 = \varphi_s^3 + 9 Ca \ln\left(\frac{x}{\lambda}\right) \quad [E.3]$$

This is the same as the small- φ_s , small- Ca limit of the model of chapter 2, the length scale λ now being determined by van der Waals forces rather than by a molecular dimension.

APPENDIX F – *The importance of inertial forces*

The ratio of the magnitude of inertial forces to that of viscous forces (in a plane wedge geometry) is given by Huh & Scriven (1971):

$$\frac{|\mathbf{v} \cdot \nabla \mathbf{v}|}{\nu |\nabla^2 \mathbf{v}|} = \frac{\rho U}{\nu} \frac{|a \sin \theta + b \cos \theta + c \theta \sin \theta + d \theta \cos \theta| \cdot |c \cos \theta - d \sin \theta|}{\sqrt{c^2 + d^2}} \quad [\text{F.1}]$$

where ν is the kinematic viscosity and \mathbf{v} the velocity field (ρ is the radial polar coordinate while the density is hidden in ν). The constants a, b, c and d have the corresponding index A or R and are as presented in appendix D. The second part of the right hand side of this equation is computed in a number of cases and presented in figures F.1 and F.2. It may be concluded that this factor is of the order 1. Thus [F.1] may be approximated as

$$\frac{|\mathbf{v} \cdot \nabla \mathbf{v}|}{\nu |\nabla^2 \mathbf{v}|} = \frac{\rho U}{\nu}. \quad [\text{F.2}]$$

A typical length scale (ρ) for the inner region seems to be $2 \cdot 10^{-5}$ m ($\xi \cong 10$ and $\lambda \cong 10^{-9}$ m) and the creeping flow approximation may be legitimate if

$$\frac{U}{\nu} << 5 \cdot 10^4 \text{ m}^{-1}. \quad [\text{F.3}]$$

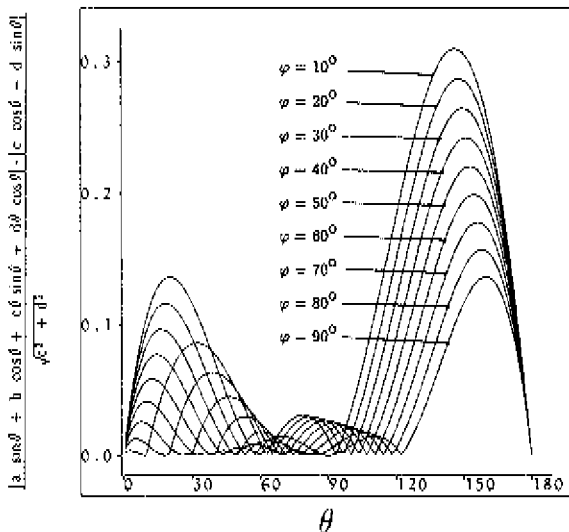


Fig. F.1 The angular dependence of the ratio of inertial forces to that of viscous forces in the case $\mu_A/\mu_R = 1$.

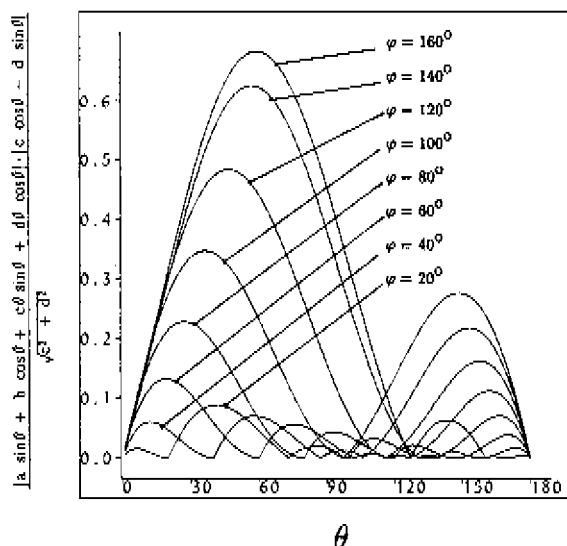


Fig. F.2 The angular dependence of the ratio of inertial forces to that of viscous forces in the case $\mu_A/\mu_R = 10^3$.

REFERENCES

- Batchelor, G.K. 1967 An introduction to fluid dynamics. Cambridge University Press.
- Blake, T.D. & Ruschak, K.J. 1979 A maximum speed of wetting. *Nature* **282**, 489–491.
- Blake, T.D. 1993 Dynamic Contact Angles and Wetting Kinetics. To be published in "Wettability", Surfactant Science Series, edited by J. Berg and published by Marcel Dekker.
- Boender, W., Chesters, A.K. & van der Zanden A.J.J. 1991 An approximate analytical solution of the hydrodynamic problem associated with an advancing liquid–gas contact line. *Int. J. Multiphase Flow* **17**, 661–676.
- Brochard, F., Redon, C. & Rondelez, F. 1988 Dewetting: the gravity controlled regime. *C. R. Acad. Sci. II* **306**, 1143–1146.
- Brochard–Wyart, F. & Daillant, J. 1990 Drying of solids wetted by thin liquid films. *Can. J. Phys.* **68**, 1084–1088.
- Brochard–Wyart, F., Meglio, J.M. & Quéré, D. 1987 Dewetting. Growth of dry regions from a film covering a flat solid or a fiber. *C. R. Acad. Sci. II* **304**, 553–558.
- Bronstein, I.N. & Semendyayev, K.A. 1973 A Guide Book to Mathematics. Verlag Harri Deutsch/Springer–Verlag.
- Cox, R.G. 1986 The dynamics of the spreading of liquids on a solid surface. Part 1. Viscous flow. *J. Fluid Mech.* **168**, 169–194.
- Dussan V., E.B. 1976 The moving contact line: the slip boundary condition. *J. Fluid Mech.* **77**, 665–684.
- Dussan V., E.B. 1979 On the spreading of liquids on solid surfaces: static and dynamic contact lines. *A. Rev. Fluid Mech.* **11**, 371–400.
- Dussan V., E.B., Ramé, E. & Garoff, S. 1991 On identifying the appropriate boundary conditions at a moving contact line: an experimental investigation. *J. Fluid Mech.* **230**, 97–116.
- Fermigier, M. & Jenffer, P. 1988 Dynamics of a liquid–liquid interface in a capillary. *Annals Phys.* **13** (2), 37–42.
- de Gennes, P.G. 1985 Wetting: statics and dynamics. *Rev. Mod. Phys.* **57**, 827–863.
- de Gennes, P.G. 1986 Deposition of Langmuir–Blodgett layers. *Colloid & Polymer Sci.* **264**, 463–465.
- de Gennes, P.G., Hua, X. & Levinson, P. 1990 Dynamics of wetting: local contact angles. *J. Fluid Mech.* **212**, 55–63.

- Greenspan, H.P. 1978 On the motion of a small viscous droplet that wets a surface. *J. Fluid Mech.* **84**, 125–143.
- Hansen, R.J. & Toong, T.Y. 1971 Interface behavior as one fluid completely displaces another from a small diameter tube. *J. Colloid Interface Sci.* **36**, 410–413.
- Hansen, R.J. & Toong, T.Y. 1971b Dynamic contact angle and its relationship to forces of hydrodynamic origin. *J. Colloid Interface Sci.* **37**, 196–207.
- Heslot, F., Cazabat, A.M. & Fraysse, N. 1989 Diffusion-controlled wetting films. *J. Phys.: Condens. Matter* **1**, 5793–5798.
- Heslot, F., Fraysse, N. & Cazabat, A.M. 1989 Molecular layering in the spreading of wetting liquid drops. *Nature* **338**, 640–642.
- Heslot, F., Cazabat, A.M. & Levinson, P. 1989 Dynamics of wetting of tiny drops: ellipsometric study of the late stages of spreading. *Phys. Rev. Lett.* **62**, 1286–1289.
- Heslot, F., Cazabat, A.M., Levinson, P. & Fraysse, N. 1990 Experiments on wetting on the scale of nanometers: Influence of the surface energy. *Phys. Rev. Lett.* **65**, 599–602.
- Hocking, L.M. & Rivers, A.D. 1982 The spreading of a drop by capillary action. *J. Fluid Mech.* **121**, 425–442.
- Hocking, L.M. 1992 Rival contact-angle models and the spreading of drops. *J. Fluid Mech.* **239**, 671–681.
- Hoffman, R.L. 1975 A study of the advancing interface I. Interface shape in liquid-gas systems. *J. Colloid Interface Sci.* **50**, 228–241.
- Hoffman, R.L. 1983 A study of the advancing interface II. Theoretical prediction of the dynamic contact angle in liquid-gas systems. *J. Colloid Interface Sci.* **94**, 470–486.
- Hopf, W. & Geidel Th. 1987 The dynamic contact angle I. Dependence of the receding contact angle on velocity in the surfactant-containing three-phase system. *Colloid & Polymer Sci.* **265**, 1075–1084.
- Huh, C. & Mason, S.G. 1977 The steady movement of a liquid meniscus in a capillary tube. *J. Fluid Mech.* **81**, 401–419.
- Huh, C. & Scriven, L.E. 1971 Hydrodynamic model of steady movement of a solid/liquid/fluid contact line. *J. Colloid Interface Sci.* **35**, 85–101.
- Kafka, F.Y. & Dussan V., E.B. 1979 On the interpretation of dynamic contact angles in capillaries. *J. Fluid Mech.* **95**, 539–565.
- Legait, B. & Sourieau, P. 1985 Effect of geometry on advancing contact angles in fine capillaries. *J. Colloid Interface Sci.* **107**, 14–20.
- Lowndes, J. 1980 The numerical simulation of the steady movement of a fluid meniscus in a capillary tube. *J. Fluid Mech.* **101**, 631–646.
- Merchant, G.J. & Keller, J.B. 1992 Contact angles. *Phys. Fluids A* **4**, 477–485.

- Moffat, H.K. 1964 Viscous and resistive eddies near a sharp corner. *J. Fluid Mech.* **18**, 1–18.
- Neogi, P. & Miller, C.A. 1982 Spreading kinetics of a drop on a smooth solid surface. *J. Colloid Interface Sci.* **86**, 525–538.
- Ngan, C.G. & Dussan V., E.B. 1984 The moving contact line with a 180° advancing contact angle. *Phys. Fluids* **27**, 2785–2787.
- Petrov, J.G. & Radoev, B.P. 1981 Steady motion of the three phase contact line in model Langmuir–Blodgett systems. *Colloid & Polymer Sci.* **259**, 753–760.
- Petrov, J.G. & Sedev, R.V. 1985 On the existence of a maximum speed of wetting. *Colloids & Surfaces* **13**, 313–322.
- Pismen, L.M. & Nir, A. 1982 Motion of a contact line. *Phys. Fluids* **25**, 3–7.
- Quééré, D. 1991 On the minimal velocity of forced spreading in partial wetting. *C. R. Acad. Sci. II* **313**, 313–318.
- Redon, C., Brochard–Wyart, F. & Rondelez, F. 1991 Dynamics of dewetting. *Phys. Rev. Lett.* **66**, 715–718.
- Rillaerts, E. & Joos P. 1980 The dynamic contact angle. *Chem. Eng. Sci.* **35**, 883–887.
- Rose, W. & Heins, R.W. 1962 Moving interfaces and contact angle rate–dependency. *J. Colloid Sci.* **17**, 39–48.
- Sedev, R.V. & Petrov, J.G. 1988/89 Influence of geometry of the three–phase system on the maximum speed of wetting. *Colloids & Surfaces* **34**, 197–201.
- Sedev, R.V. & Petrov, J.G. 1991 The critical condition for transition from steady wetting to film entrainment. *Colloids & Surfaces* **53**, 147–156.
- Teletzke, G.F., Davis, H.T. & Scriven L.E. 1988 Wetting hydrodynamics. *Rev. Phys. Appl.* **23**, 989–1007.
- Thompson, P.A. & Robbins, M.O. 1989 Simulations of contact–line motion: slip and the dynamic contact angle. *Phys. Rev. Lett.* **63**, 766–769.
- Thompson, P. & Robbins, M. 1990 To slip or not to slip? *Physics World*, november 1990, 35–38.
- Tilton, J.N. 1988 The steady motion of an interface between two viscous liquids in a capillary tube. *Chem. Eng. Sci.* **43**, 1371–1384.
- Voinov, O.V. 1976 Hydrodynamics of wetting. *Fluid Dynam.* **11**, 714–721.
- Voinov, O.V. 1978 Asymptote to the free surface of a viscous liquid creeping on a surface and the velocity dependence of the angle of contact. *Sov. Phys. Dokl.* **23**, 891–893.
- Zhou, M–Y. & Sheng, P. 1990 Dynamics of immiscible–fluid displacement in a capillary tube. *Phys. Rev. Lett.* **64**, 882–885.

SUMMARY

A contact line is formed where an interface between two immiscible fluids intersects a solid surface. In the ideal static case the angle between the interface and the wall is a material property and is called the static contact angle. If the contact line is forced to move over the solid surface the dynamic contact angle is a function of the line speed. Computations have shown, however, that the change of the contact angle is, at least partially, apparent. The shape of the interface deviates close to the contact line strongly from the macroscopic observable profile due to viscous forces in the fluids.

In this thesis a model has been developed to predict the shape of a meniscus moving between parallel planes or inside a capillary tube in the case in which inertial forces may be neglected. The model, which is based on a local-wedge approximation, results in a second-order ordinary differential equation which is integrated numerically. The results compared closely with available full numerical solutions.

In order to avoid a singularity at the contact line the model must lose its validity close to the wall. The boundary conditions at the wall are modelled by putting forward that at a very small distance (λ) from the wall, where the continuum description loses its validity, the final meniscus inclination, called the true contact angle (φ_0), is reached. The parameters λ and φ_0 are subsequently evaluated by comparison with experiments.

The model is applied in the cases where a viscous liquid displaces a fluid with a negligible viscosity, an 'advancing' contact line, where a viscous liquid is being displaced by a fluid with a negligible viscosity, a 'receding' contact line, and in the case a moving interface is formed between two viscous liquids.

From the comparison of the present model with experiments reported in the literature and reported here it is concluded that λ is indeed of the order of a molecular

dimension and that the true contact angle can in some cases sufficiently be approximated by the static contact angle while in other cases a clear line-speed dependence can be observed. It is not clear what causes this dependence.

Finally the shape of an advancing meniscus inside a capillary tube has been measured with a light reflection technique up to about $5 \cdot 10^{-8}$ m from the wall. These measurements show the shape of the major part of the meniscus where it deviates from the spherical. Aside from a small systematic deviation these measurements confirm the model.

SAMENVATTING

Waar een scheidingsvlak tussen twee niet mengbare fluida een vaste wand raakt bevindt zich een contactlijn. De hoek, welke het scheidingsvlak maakt met de wand, is in het ideale, statische geval een materiaalconstante en wordt de statische contacthoek genoemd. Indien nu de contactlijn gedwongen wordt over de vaste wand te lopen is de dynamische contacthoek een functie van de lijnsnelheid. Berekeningen hebben echter aangetoond dat de verandering van de contacthoek, in ieder geval grotendeels, schijnbaar is. Ten gevolge van de visceuse krachten in de vloeistof wijkt de vorm van het scheidingsvlak dicht bij de contactlijn sterk af van het macroscopisch zichtbare profiel.

In dit proefschrift is een model ontwikkeld om de vorm van een meniscus, die zich tussen twee parallele platen of in een capillair verplaatst, te kunnen voorspellen in het geval dat traagheidskrachten verwaarloosd mogen worden. Het model, dat gebaseerd is op een lokale wigbenadering, resulteert in een tweede orde, gewone differentiaal vergelijking voor de vorm van de meniscus, welke numeriek opgelost wordt. De resultaten komen vrij goed overeen met beschikbare, volledige, numerieke oplossingen.

Om een singulariteit aan de contactlijn te voorkomen moet het model ophouden geldig te zijn ergens dicht bij de wand. De randvoorwaarden aan de wand worden gemodelleerd door te zeggen dat op een zeer kleine afstand (λ) tot de wand, waar de continuum benadering zijn geldigheid verliest, de uiterste meniscushelling, de werkelijke contacthoek (φ_0) genoemd, bereikt is. De parameters λ en φ_0 zijn vervolgens bepaald door vergelijkingen met experimenten.

Het model is toegepast in het geval een visceuse vloeistof een fluidum met een verwaarloosbare viscositeit verdringt, een 'voortuitlopende' contactlijn, in het geval een visceuse vloeistof verdrongen wordt door een vloeistof met een verwaarloosbare viscositeit,

een 'terugtrekkende' contactlijn, en in het geval een bewegend scheidingsvlak gevormd wordt tussen twee visceuse vloeistoffen.

Uit de vergelijking van het model met experimenten uit de literatuur en verricht in de kader van dit onderzoek is geconcludeerd dat λ inderdaad van de orde van een moleculaire afmeting is en dat de werkelijke contacthoek in sommige gevallen benaderd kan worden met de statische contacthoek terwijl in andere gevallen er een duidelijke afhankelijkheid van de lijnsnelheid waargenomen wordt. Het is niet duidelijk waardoor deze afhankelijkheid veroorzaakt wordt.

Tenslotte is met behulp van een lichtreflectiemethode de vorm van een vooruitlopende meniscus in een capillair gemeten tot ongeveer $5 \cdot 10^{-8}$ m van de wand. Deze metingen tonen de vorm van het overgrote gedeelte van de meniscus dat afwijkt van de bolvorm. Op een kleine systematische afwijking na bevestigen deze metingen het model.

CURRICULUM VITAE

- 3-9-1964 Born in Helmond (the Netherlands) as son of Leonardus Antonius van der Zanden and Hendrika Adriana van der Zanden-Maas.
- 2-6-1982 Gymnasium Diploma, Deurne (the Netherlands).
- 22-6-1988 Engineering degree (Physics) Eindhoven University of Technology.
- 1-7-1988 till 1-7-1992
- Ph.D. research student at the Eindhoven University of Technology, at the Laboratory of Fluid Dynamics and Heat Transfer (Physics Department).

NAWOORD

Op de eerste plaats ben ik heel veel dank verschuldigd aan mijn eerste promotor, Allan Chesters. Tijdens de afgelopen 4 jaren heb ik hem leren ervaren als een energieke en stimulerende wervelwind, die met zijn vakkennis en creativiteit op een krachtige wijze het onderzoek heeft begeleid. Ik waardeer zijn manier van begeleiden ten zeerste, met name de ruimte die er altijd was om op eigen wijze onderzoek te doen en om fouten te mogen maken. Allan bedankt.

Ook ben ik veel dank verschuldigd aan Pim Sluyter. Ik heb veel profijt gehad van zijn technisch inzicht en zijn kennis omtrent de organisatorische wegen binnen de universiteit als er weer eens iets gemaakt moest worden. Ik denk dat hij er voor een groot gedeelte aan bijgedragen heeft dat de experimenten zo soepeltjes verlopen zijn. Pim bedankt.

Verder bedank ik alle andere mensen die bijgedragen hebben aan de totstandkoming van dit proefschrift.

Tenslotte wil ik er op wijzen dat de wetenschappelijke kennis die hier vergaard is niet het enige product is van dit promotieonderzoek. Ik zelf ben namelijk eveneens gedeeltelijk een product van dit promotieonderzoek. Ik heb geleerd, uitgaande van de aanvaarde vooronderstellingen, de dingen objectief te onderzoeken en minder snel met een eigen mening klaar te staan. Dit is ook in het dagelijks leven vaak heel nuttig. Want, zo zegt Ouspensky, "We must realize how often we are governed and controlled not by things themselves but by our own ideas of things, our views of things, our picture of things!"

¹P. D. Ouspensky in *The Fourth Way*. Published by Penguin/Arkana.

Stellingen behorende bij het proefschrift van A.J.J. van der Zanden, Eindhoven, 5-1-1993.

1. De singulariteit aan een bewegende contactlijn, welke gevonden wordt indien de gebruikelijke hydrodynamische wetten gehandhaafd blijven, wordt vermeden door het moleculaire karakter van de betrokken materialen.

Dit proefschrift

2. De aanpak van het invoeren van een "sliplengte" ter vermindering van de singulariteit aan een bewegende contactlijn suggereert ten onrechte kennis over de precieze physica aan de contactlijn.
3. De werkelijke dynamische contacthoek is niet noodzakelijkerwijs gelijk aan de statische contacthoek maar kan een functie zijn van de snelheid van de contactlijn.

Dit proefschrift

M-Y. Zhou & P. Sheng, Phys. Rev. Lett, 64, 882-885

4. Totdat de invloed van surfactants en wandruwheid op een bewegende contactlijn in kaart gebracht is moet een vergelijking van een experiment met een theorie, waarbij uitgegaan wordt van surfactant vrije systemen en gladde oppervlakken, altijd met enige terughoudendheid benaderd worden.
5. Door kinderen voor straf langer op school te laten blijven wordt hen geleerd de school niet leuk te vinden.
6. Om bij de huidige opkomstpercentages bij landelijke verkiezingen in Nederland te gaan stemmen met het doel de uitslag te beïnvloeden, is, voor een individu, statistisch gezien, onzin.

7. Luiheid is een goede eigenschap mits deze gepaard gaat met intelligentie en/of wijsheid.
8. Ten onrechte beschouwen de meeste mensen hun lichaam als zijnde *van* hen terwijl zij hun bloed beschouwen als zijnde *in* hen.
9. Televisie/krant is opium voor het volk.
10. Een kenmerk van fanatisme is dat het zichzelf vernietigt.